AEROSPACE REPORT NO.
ATR-2005(5131)-1

Quantitative Evaluation of Flaw-Detection Limits of Eddy Current Techniques for Interrogating Structures Beneath Thermal Protection Systems on Reusable Launch Vehicles

25 February 2005

Prepared by

O. ESQUIVEL and Y. M. KIM
Space Materials Laboratory
Laboratory Operations

Prepared for

VOLPE NATIONAL TRANSPORTATION SYSTEMS CENTER
U.S. DEPARTMENT OF TRANPORTATION
Cambridge, MA 02142

Contract No. DTRS57-99-D-00062
Task 8.0

Space Launch Operations

PUBLIC RELEASE IS AUTHORIZED

THE AEROSPACE CORPORATION
EL SEGUNDO, CALIFORNIA

Technical Report Documentation Page

1. Report No. DOT-VNTSC-FAA-05-02	**2. Government Accession No.**	**3. Recipient's Catalog No.**
4. Title and Subtitle Quantitative Evaluation of Flaw-Detection Limits of Eddy Current Techniques for Interrogating Structures Beneath Thermal Protection Systems on Reusable Launch Vehicles		**5. Report Date** February 25, 2005 **6. Performing Organization Code** DOT-RITA-VNTSC-DTS-67
7. Author(s)* O. Esquivel and Y. M. Kim		**8. Performing Organization Report No.**
9. Performing Organization Name and Address U.S. Department of Transportation Research and Innovative Technology Administration Volpe National Transportation Systems Center Aviation Safety Division Cambridge, MA 02142-1093		**10. Work Units No. (TRAIS)** FA2R; BL411 **11. Contract or Grant No.**
12. Sponsoring Agency Name and Address U.S. Department of Transportation Federal Aviation Administration Office of the Assoc. Administrator for Commercial Space Transportation Washington, DC 20591		**13. Type of Report and Period Covered** Contractor Final Report: April – December 2004 **14. Sponsoring Agency Code** FAA/AST-300

15. Supplementary Notes

*The Aerospace Corporation, El Segundo, CA 90245-4691, under contract to the Volpe National Transportation Systems Center -- Contract No. DTRS57-99-D-00062, Task 8.

Aerospace Corporation Report No. ATR-2005(5131)-1

16. Abstract

The Aerospace Corporation (Aerospace) was tasked by the Volpe National Transportation Systems Center to provide technical support to the Federal Aviation Administration, Office of Commercial Space Transportation (FAA/AST), to quantitatively evaluate flaw detection limits of eddy current techniques for interrogating structures beneath thermal protection systems (TPSs) on reusable launch vehicles (RLVs). A quantitative study was performed to identify the nominal flaw detection limits for selected nondestructive evaluation (NDE) methods applied to RLV structures covered by TPS.

This effort focused on the application of eddy current techniques. The primary elements of this task were: (1) Obtain or fabricate two substrate material systems simulating families of RLV structures (structural alloy and graphite/epoxy composite) with varying degrees of flaw-size damage (machine notches, delaminations, impacts). Cover each substrate with an actual or simulated TPS coating of varying thickness. (2) Use eddy current NDE methods to assess the minimum detectable flaw (size and/or depth) in each material system as a function of TPS thickness. (3) Assess potential areas where advanced development may enhance the limits of detection pertaining to RLV/TPS applications (probe design, advanced signal processing, etc).

This task provided a quantitative assessment of the capabilities of eddy current methods in materials that closely represent those of suborbital RLV configurations. This NDE technique was successfully studied on systematically simulated RLV flaw standards in order to understand the technique's benefits and limitations and the potential for advances in its development to fulfill future needs of RLV developers.

17. Key Words Reusable Launch Vehicle, RLV, Nondestructive Evaluation, NDE, Eddy Current, Thermal Protection System, TPS, Licensing, Regulation		**18. Distribution Statement** PUBLIC RELEASE IS AUTHORIZED.	
19. Security Classification. (of this report) None	**20. Security Classification. (of this page)** None	**21. No. of Pages** 48	**22. Price**

Form DOT F 1700.7 (8-72) **Reproduction of completed page authorized**

AEROSPACE REPORT NO.
ATR-2005(5131)-1

QUANTITATIVE EVALUATION OF FLAW-DETECTION LIMITS OF EDDY CURRENT TECHNIQUES FOR INTERROGATING STRUCTURES BENEATH THERMAL PROTECTION SYSTEMS ON REUSABLE LAUNCH VEHICLES

Prepared by

O. ESQUIVEL and Y. M. KIM
Space Materials Laboratory
Laboratory Operations

25 February 2005

Space Launch Operations
THE AEROSPACE CORPORATION
El Segundo, CA 90245-4691

Prepared for

VOLPE NATIONAL TRANSPORTATION SYSTEMS CENTER
U.S. DEPARTMENT OF TRANPORTATION
Cambridge, MA 02142

Contract No. DTRS57-99-D-00062
Task 8.0

PUBLIC RELEASE IS AUTHORIZED

AEROSPACE REPORT NO.
ATR-2005(5131)-1

QUANTITATIVE EVALUATION OF FLAW-DETECTION LIMITS OF EDDY CURRENT TECHNIQUES FOR INTERROGATING STRUCTURES BENEATH THERMAL PROTECTION SYSTEMS ON REUSABLE LAUNCH VEHICLES

Prepared by:

O. Esquivel
Materials Processing and Evaluation Department

Y. M. Kim
Materials Processing and Evaluation Department

Approved by:

E. C. Johnson, Associate Director
Materials Processing and Evaluation Department
Space Materials Laboratory
Laboratory Operations

E. K. Ruth, Systems Director
Commercial Launch Systems
Space Launch Support Division
Space Launch Operations

Contents

Abstract ix

Acknowledgments xi

1. Introduction and Summary 1

2. Overview and Background 3

2.1 Inspection Equipment 3

2.2 Eddy Current Techniques 4

2.3 Advantages and Disadvantages 7

2.4 General Applications to TPS Configurations 8

3. Study of Detection Limits for TPS Covered Structures 9

3.1 Selection and Fabrication of Candidate Material Systems 9

3.2 Material Flaw Configurations 10

3.2.1 EDM Notches in Alloy Substrates 10

3.2.2 Alternate Crack Fabrication Approaches 11

3.2.3 Impact Damage in G/E Composite Substrates 14

3.3 Approach and Application of Eddy Current Inspection Technique 18

3.4 Results Obtained for Limits of Detection with TPS Thickness 24

3.4.1 Results of Limits of Detection for Composite Specimens 29

3.5 Directions for Advanced Development 31

4. Summary of Results 37

5. Conclusions and Recommendations 39

6. Abbreviations and Symbols 41

7. References 43

Figures

Figure 2-1. Examples of probe coil configurations: Pancake probe for flat surfaces and solenoid coil for tubular parts. Source: Ref. 2; used by permission. 4

Figure 2-2. Pattern of eddy current in a "good" part, versus disruption of eddy currents in presence of a crack. Source: Ref. 2; used by permission..... 4

Figure 2-3. Representation of distortion of eddy current field as function of specimen thickness. Source: Ref. 2; used by permission. 5

Figure 2-4. Standard penetration depth as function of frequency for selected materials. Source: Ref. 2; used by permission. 6

Figure 2-5. Vector point representation of coil impedance changes in eddy current inspection. (a) Impedance plane display on oscilloscope. (b) Vector point traces showing conductivity response. (c) Point traces for defect indications. Source: Ref. 2; used by permission. 7

Figure 3-1. Substrates consisting of 6061-T6 Al plate and graphite/epoxy composite sheet; simulated TPS represented by thin cork sheet overlays of varying thickness. 10

Figure 3-2. EDM notches produced on two 4 in. x 4 in. x 1/8 in. thick 6061-T6 aluminum plates..... 11

Figure 3-3. Sequence of steps to fabricate a closed "crack-like" flaw by a rejoining method..... 12

Figure 3-4. Example of filled-joint technique for creating fine crack-like flaws for subsequent eddy current detection. This trial was made using a copper substrate and SnPb solder as the filler material (left). Crack detection was successful above 2 layers of 1/16-in. thick cork (right)..... 12

Figure 3-5. Schematic diagram of split-plate coupon with variable crack width. Coupons were made with an initial crack width of 0.020 inches. Silicone adhesive allows plates to be compressed in a vise to achieve a completely closed crack..... 13

Figure 3-6. Example of split-plate coupon in test set-up vise prior to eddy current inspection measurement. Left, fully open crack (0.020-in.), right, completely closed crack. 14

Figure 3-7. Variable split-plate coupons representing three different surface crack depths. The thickness of the upper plates (0.090, 0.048, 0.018-in.) define the crack depth. 14

Figure 3-8. Instrumented impact testing machine used to create flaws in composite specimens. 15

Figure 3-9. View of composite specimen support apparatus within impact testing rig..... 16

Figure 3-10. Front and rear surfaces of composite specimens with impact damage. Impact energies (from left) 136.1, 90.7, 79.4, 68.0, 45.4 in-lbs. Note: no discernable damage at lowest level impact; distinct damage threshold between 68.0 and 79.4 in-lbs; small change in magnitude of damage from 79.4 to 136.1 in-lbs. 17

Figure 3-11. Images obtained with infrared flash thermography showing indications of the extent of internal delaminations (light areas) in two of the impacted composite specimens. 18

Figure 3-12. Portable eddy current test unit (Zetec MIZ-22) typical of common field instruments optimized for a variety of inspection applications. Typical variety of search coil probes used on flat targets. 19

Figure 3-13. Example of inspection setup for detection of defects on bare substrate and with incremental TPS thickness (multiple cork sheets). 19

Figure 3-14. Schematic and actual data obtain from an eddy current probe scan over a closed crack in a fatigue specimen of Ti-6Al-4V. The plots show the trace of the impedance change produced by the presence of the crack as well as the effect of slight probe lift-off. Note: units scaling in all impedance plots is abritrary. 20

Figure 3-15. Photo of metal conductivity standard and results of coil/target impedance change measured with the eddy current probe at the surface of each metal. 21

Figure 3-16. Eddy current response for closed fatigue crack in Ti-6Al-4V follows the conductivity path between the titanium alloy and a graphite (lower conductivity) specimen. 21

Figure 3-17. Change in eddy current response signal as probe is scanned over a tightly closed crack verses cracks with of equal depth but greater width. 22

Figure 3-18. Eddy current inspection set-up. Support structure for probe on micrometer control stage to adjust probe height (TPS thickness). Split-plate coupon, held within vise to adjust crack width opening, mounted on scanning translation stage. 23

Figure 3-19. Schematic and actual data obtain from inspection standard of equal width grooves of varying depths. 23

Figure 3-20. Schematic and actual data obtain from inspection standard of equal width grooves of varying depths. 24

Figure 3-21. Issues identified which may cause spit-plate coupon response to deviate from a real surface crack. Left, base/split-plate interface contributes to response signal; right, thin plates (shallow cracks) deflect upwards with clamp pressure. 25

Figure 3-22. Variation in signal magnitude with probe lift-off distance for 0.018-in deep, closed surface crack. The change in signal strength shows the relative affect of increasing TPS thickness. 26

Figure 3-23. Results comparing the response of the EDM notches at two different depths, 0.045-in and 0.067-in deep. Both notches are 0.025-in. wide. For both specimens the notch length was 0.25 inches. Similar results were obtained for notches of 0.50 length due to the small diameter pencil probe used in the measurements. 27

Figure 3-24. Variation in signal magnitude with probe lift-off distance for EDM notch 0.067-in deep, 0.025 wide. The change in signal strength shows the relative affect of increasing TPS thickness. 27

Figure 3-25. Results of lift-off sensitivity measurements. Magnitude of eddy current signal response with probe lift-off height shown as a percentage of signal obtain at surface (zero lift-off). 28

Figure 3-26. Results of scan on undamaged composite (left) and the response due to probe lift-off. 29

Figure 3-27. Results of two orthogonal surface scans on most heavily impacted composite specimen. Some surface tilt indicated as a change in lift-off distance from scan start to finish point. 29

Figure 3-28. Attenuation in signal with probe lift-off increase from 0.08 inches to 0.12 inches on the most heavily impacted specimen. 30

Figure 3-29. Attenuation in signal with probe lift-off increase from zero inches (surface) to 0.04 inches on the specimen which showed barely discernable damage (68.0 in-lb). 31

Figure 3-30. Laboratory components assembled for investigative EC/material response studies. This setup provides EC flaw detection capabilities similar to the commercial unit but allows greater latitude in signal analysis, data processing, probe design, and response modeling. Emphasis is on material properties evaluation as well as flaw detection. 32

Figure 3-31. By measuring frequency-dependant complex impedance, the influence of the sample with and without a flaw is manifested in a shift in the resonance frequency and a change in the width of resonance. 33

Figure 3-32. Presentation of eddy current signal response plotted as resonant frequency and frequency width, derived from swept-frequency impedance measurements. Systematic effects of conductivity variations and probe lift-off distance are clearly evident and can be extrapolated. 34

Figure 3-33. Enlargement of plot shown in prior figure. Scatter in measurement data will be important in defining the limit in liftoff or TPS thickness that can be sustained and still resolve the signal produced by the flaw. 34

Figure 3-34. Contrast of coil design used in typical pencil probes (left) and horseshoe core that induces directional eddy currents that can be used to discriminate the orientation of specific flaws. 35

Figure 3-35. Laboratory constructed horseshoe probes used in the development of alternate eddy current approaches. 36

Abstract

The Aerospace Corporation was tasked by the Volpe National Transportation Systems Center to provide technical support to the Federal Aviation Administration, Office of Commercial Space Transportation (FAA/AST), to quantitatively evaluate flaw detection limits of eddy current techniques for interrogating structures beneath thermal protection systems (TPSs) on reusable launch vehicles (RLVs). A quantitative study was performed to identify the nominal flaw detection limits. The primary elements of this task were: (1) Obtain or fabricate two substrate material systems simulating families of RLV structures (structural alloy and graphite/epoxy composite) with flaws of various defined sizes (machine notches, delaminations, impacts). Cover each substrate with an actual or simulated TPS coating of varying thickness. (2) Use eddy current NDE methods to assess the minimum detectable flaw (size and/or depth) in each material system as a function of TPS thickness. (3) Assess potential areas where advanced development may enhance the limits of detection pertaining to RLV/TPS applications (probe design, advanced signal processing, etc). This task provided a quantitative assessment of the capabilities of eddy current methods in materials that closely represent those of suborbital RLV configurations. This NDE technique was successfully studied on systematically simulated RLV flaw standards in order to understand the technique's benefits and limitations and the potential for advances in its development to fulfill future needs of RLV developers.

Acknowledgments

Dr. Oscar Esquivel and Robert W. Seibold served as Principal Investigator and Program Manager, respectively. Dr. Yong M. Kim is performing the laboratory experimentation. The authors are grateful for the valuable guidance and support provided by the following Aerospace personnel: Dr. James P. Nokes and Dr. Eric C. Johnson.

Gratitude is extended to Mr. Jamil (Jim) Kabbara at the Office of the Associate Administrator for Commercial Space Transportation, Federal Aviation Administration, for valuable guidance on FAA/AST regulatory and licensing needs. The authors also wish to thank Mr. John J. Sigona, who served as the Contracting Officer's Technical Representative (COTR) at the Volpe National Transportation Systems Center and provided valuable insight on government needs and regulations.

1. Introduction and Summary

The need to assure the health and flightworthiness of reusable launch vehicle (RLV) structures is a fundamental concern for the success and safety of future commercial space launch ventures. Critical to achieving this assurance are the myriad material- and component-level inspection processes performed throughout the manufacturing, testing, and service life of these flight hardware systems. Among the most vital inspection processes are nondestructive evaluation (NDE) methods used for evaluating the quality of flight structures. The NDE methods enable inspection without damaging or degrading the inspected parts.

Several NDE techniques are suitable for subassembly inspections; however, options narrow as material systems and subassemblies are integrated and accessibility for inspection becomes limited. Accessibility is particularly relevant to RLV flight structures covered with thermal protection systems (TPSs). Thermal protection systems provide necessary thermal barriers against harsh environments imposed during reentry or by other operational heat loads. As the external skin of the vehicle, TPSs play a crucial role in protecting critical structural elements. The design and capabilities of TPSs vary with location and vulnerability of the underlying structure. Various material systems may be used for TPSs, such as ablative or durable insulation coatings, bonded or sprayed multilayers, flexible blankets, or ridged refractory tiles. All of these TPS types can constrain access to the underlying structures for inspection. In some cases, removal and reapplication of the TPS may be required to inspect these structures. Where direct access to critical flight structures is unavailable or impractical, inspection processes that can detect substrate flaws beneath the TPS are needed.

Under a previous study, a brief descriptive summary of various NDE methods relevant to the inspection of launch vehicle structures covered by TPS was provided (Ref. 1). Basic issues affecting the inspection of structures protected by TPS were identified, and the inherent strengths and limitations of the various NDE techniques as they relate to the projected needs of future RLV systems were described. An understanding of present NDE capabilities also served to aid identification and guide development of advanced NDE techniques offering improved potential for inspection of future RLV structures. Under that study, eddy current techniques, among others, were identified as a promising approach for the present study. Some specific issues associated with eddy current techniques are discussed in Section 2.

2. Overview and Background

Eddy current inspection techniques are based on the generation or induction of electrical eddy currents in a workpiece and understanding how these eddy currents respond to the presence of flaws or changes in material conditions. Since the method is based on electromagnetic induction, the target materials must be electrically conducting to some degree and are most often metals, structural alloys, or graphite fiber composites. Eddy current methods are highly versatile and can be used to detect surface and subsurface cracks, voids, inclusions, and effects of corrosion. This technique can be used to assess material thickness or thickness variations in surface coatings, as well as changes in electrical conductivity, grain size, hardness, heat treatment conditions, and a variety of other compositional and microstructural conditions. Since the eddy currents are induced by the proximity of a probe coil, direct contact with the workpiece is not required. Thus, the technique can be adapted to automated, high-speed scanning configurations, or where non-contact methods are desired due to contamination sensitivity. Because the eddy current signal response (monitored as the change in probe coil impedance) is sensitive to a wide range of structural, physical, and geometrical characteristics, one important concern is the ability to distinguish flaw-related signal changes from those due to other non-flaw, material variables. This, however, can be addressed through appropriate inspection development procedures and the use of suitable material defect standards.

2.1 Inspection Equipment

The equipment for performing eddy current inspection can vary in complexity, but typically consists of (1) a search coil probe element, which, when energized with an AC current, induces eddy currents in a conductive workpiece; (2) a variable-frequency voltage generator to excite the search coil (typically within the frequency range of 1 kHz to 5 MHz for nonmagnetic materials and at lower frequencies for ferromagnetics); (3) a phase-sensitive voltage detector to measure coil impedance change induced by the eddy currents in the presence of defects; and (4) an x-y oscilloscope for the phasor display of coil impedance change (or other representations of the response signal). The generation, detection, and display electronics are typically incorporated into a portable eddy current inspection unit to which various types of hand-held inspection coil probes can be attached depending on the nature of the inspection (described in further detail below). Commonly, variations of these basic functions are incorporated into line-production, fixed-station inspection units for tubing fabrication, or other continuous manufacturing inspection applications.

While the basic instrumentation required for performing eddy current inspection is relatively straightforward, proper interpretation of the response signals requires careful consideration of inspection parameters such as probe alignment relative to the test surface, probe contact or liftoff consistency, and appropriate selection of setup parameters (excitation frequency, probe configuration, etc). Specially designed probe fixtures and appropriate material defect standards that emulate the maximum allowable flaw size should not be overlooked as essential elements for eddy current inspection.

2.2 Eddy Current Techniques

When a coil carrying an alternating current is placed in proximity to a conductive material, eddy (or circular) currents are induced within the material. These induced currents produce a magnetic field that is in opposition to the primary magnetic field surrounding the coil (Lenz's law). This interaction between fields causes a back electromagnetic force (emf) in the coil and, thus, a change in the coil impedance value. If a material is uniform in composition and dimensions, the impedance value of the probe or search coil placed close to the surface should be the same at all points on the surface. If the material contains a discontinuity (surface or subsurface crack), the distribution and magnitude of the eddy currents will be altered in the vicinity of the discontinuity. With this change, there will be a consequent reduction in the magnetic field associated with the eddy currents, so the coil impedance value will be altered. Two of the more common configurations of search coils are the flat or pancake type coil used to examine flat surfaces and the solenoid type coil used to surround cylindrical parts or inserted in a bore of tubing (Figure 2-1). A schematic representation of the effect of a discontinuity on the eddy current pattern is shown in Figure 2-2.

Sometimes two or more search coil elements may be employed, where one functions as a driver to induce eddy current and another to detect (reflection probe). In an "absolute" configuration, one coil samples a "good" reference specimen, while a differential signal is created with an identical coil on a test specimen. To eliminate non-defect-related variables, two adjacent coils may be used to compare

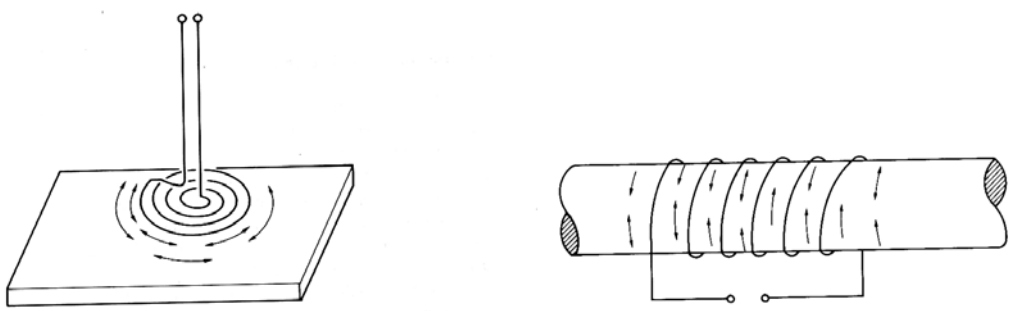

Figure 2-1. Examples of probe coil configurations: Pancake probe for flat surfaces and solenoid coil for tubular parts. Source: Ref. 2; used by permission.

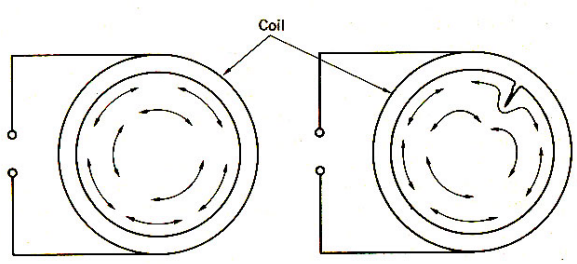

Figure 2-2. Pattern of eddy current in a "good" part, versus disruption of eddy currents in presence of a crack. Source: Ref. 2; used by permission.

regions on the same part. This "differential" configuration is insensitive to common variables (i.e., gradual dimensional variations), while abrupt discontinuities (cracks) will be very apparent under each coil scan.

The electrical conductivity of a material is one of the major parameters in eddy current testing. Because the resulting coil impedance is a strong function of material conductivity, any material condition that affects conductivity may also be monitored by the eddy current response. Minor variations in alloy chemistry, cold working, heat treatment, and surface temperature will influence eddy current response. Changes in material hardness can often be discriminated using eddy current inspection.

Because eddy currents are induced by a varying magnetic field, the magnetic permeability of a material strongly influences the eddy current response. In non-ferromagnetic materials, the secondary electromagnetic field is derived solely from the induced eddy currents. In ferromagnetic materials (some steels and alloys of iron, nickel, and cobalt), the additional magnetic effects, due to their variable and high relative magnetic permeability, are of sufficient magnitude to overshadow the field effects produced by eddy currents. However, by magnetizing ferromagnetic parts to saturation (constant permeability), these effects can be minimized. Inspection of magnetic materials is typically performed within a magnetizing coil carrying direct current of a value to achieve saturation.

The distribution of eddy currents induced within a part by the probe coil decreases exponentially with distance from the surface. This "skin effect" is typically quantified by a parameter called the standard penetration depth, S, which is a function of the material resistivity and magnetic permeability, and the frequency of the excitation current. Figure 2-3 depicts distortion of the eddy current field with

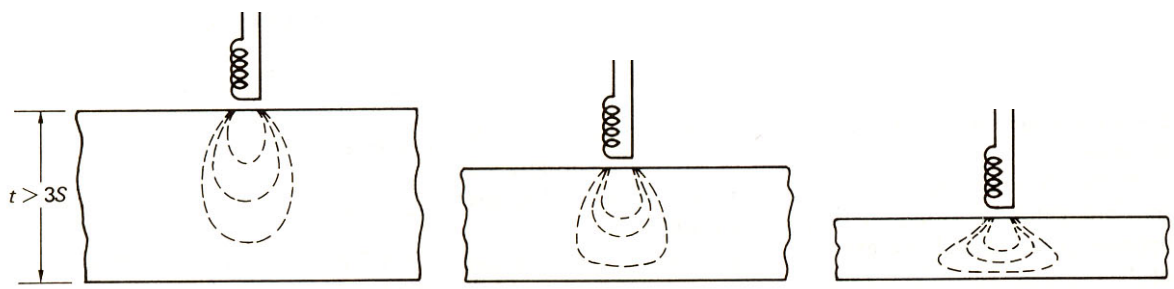

Figure 2-3. Representation of distortion of eddy current field as function of specimen thickness. Source: Ref. 2; used by permission.

specimen thickness. For relatively "thin" sections, the change in coil impedance with eddy current distortion may be calibrated as a thickness indicator (if all other influences on eddy currents remain constant). For sections roughly greater than three times the standard penetration depth, the eddy currents are no longer affected by the back surfaces. The standard penetration depth as a function of frequency is shown for selected materials in Figure 2-4.

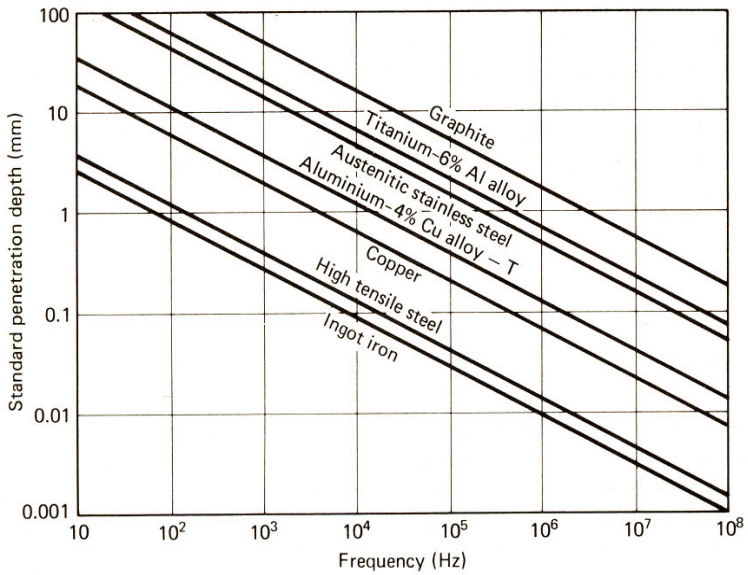

Figure 2-4. Standard penetration depth as function of frequency for selected materials. Source: Ref. 2; used by permission.

Cracks and other sharp discontinuities in a material are typically indicated by the abrupt displacement of a vector point or spot on an oscilloscope display screen. The position of the spot represents the magnitude and phase relationship of the coil "impedance" at the fixed operating frequency. To achieve this, typically under constant AC current, the complex voltage drop across the probe is measured. Doing so, the measured voltage will be proportional to the impedance. As the coil impedance changes with proximity to the surface (lift-off distance), proximity to the material edge (edge effects), or changes in other material properties, the position of the spot will trace a well-defined, systematic trajectory across the scope screen. With the appropriate selection of excitation frequency and coil design, flaw-related signal changes can be distinguished from non-flaw-induced changes (usually by displacement direction). The unique trace of the vector point on the screen caused by a specific type of flaw, material conductivity, lift-off distance, or other characteristics can be calibrated with the aid of appropriately fabricated material standards. Examples of these types of displays are shown in Figure 2-5.

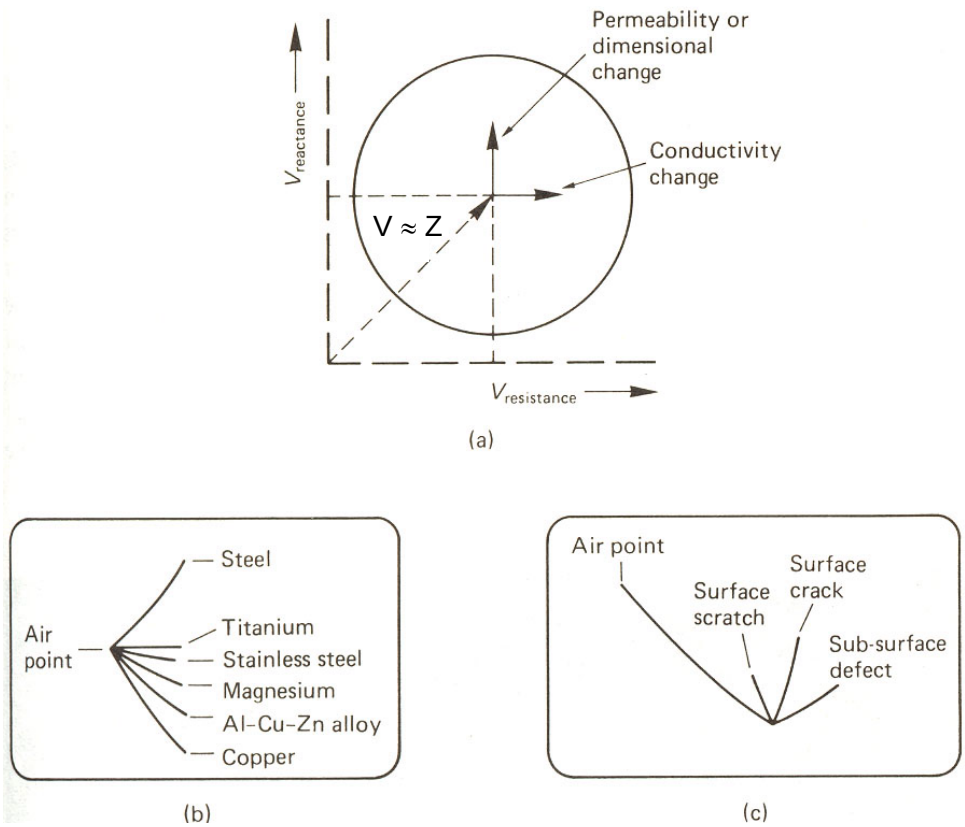

Figure 2-5. Vector point representation of coil impedance changes in eddy current inspection. (a) Impedance plane display on oscilloscope. (b) Vector point traces showing conductivity response. (c) Point traces for defect indications. Source: Ref. 2; used by permission.

2.3 Advantages and Disadvantages

The general advantages of eddy current inspection as compared to other NDE methods include:

- Sensitive to very fine surface and subsurface flaws, cracks, defects.
- Can be performed without surface contact.
- Can be used to assess thickness, conductivity, microstructural changes.
- Can inspect “beneath” nonmetallic surface coatings and overlays.
- Portable, adaptable to field use.

Disadvantages include:

- Single-point measurement. Probe must scan or raster to cover surface area.
- Inspection applicable only to electrically conducting materials (metals, alloys, graphite composites).

- Limited depth penetration. Skin effect (lower frequency increases penetration depth but with less sensitivity to flaws).
- Sensitivity to edge effects. Inspection must exclude regions near edges.
- Defect-related signals must be distinguished from signals caused by other material characteristic changes.

2.4 General Applications to TPS Configurations

Because eddy current techniques are based on electromagnetic induction, they offer some capability, in principle, for the inspection of a metallic structure covered by, or buried beneath, a nonmetallic coating. The induction of eddy current is primarily a function of the target material's electrical conductivity, magnetic permeability, and proximity. Since no force or electrical signals are directly conducted from the sensor to the target, an air gap, or intervening layer of nonconductive material may be imposed between the probe coil and the surface. Typically, the eddy current lift-off response (sensitivity to proximity of the test surface) is useful for calibrating the thickness of paint, anodized coatings, or other thin layers. If the uniformity of the coating layer is not a strong variable, eddy current detection for hidden cracks in the substrate, beneath the coating, remains viable. As the coating thickness increases, however, the sensitivity of the eddy current response to substrate flaws will diminish. Several operational parameters may be tailored to optimize the response with increasing lift-off. The use of lower frequencies is the most direct approach. Probe design with effective coil shielding can shape the magnetic flux field for optimum directionality. Although it is difficult to ascribe absolute limits on crack detection sensitivity beneath coating layers for a generic material system, the potential for developing eddy current-based NDE techniques to specific RLV TPS configurations is promising.

3. Study of Detection Limits for TPS Covered Structures

A quantitative study was undertaken to identify the nominal flaw detection limits for general eddy current inspection methods applied to RLV structures covered by TPS. The primary elements of this study were:

1. Obtain or fabricate two substrate material systems simulating families of RLV structures (structural alloy and graphite/epoxy composite) with flaws of various defined sizes (machine notches, delaminations, impacts).
2. Cover each substrate with an actual or simulated TPS coating of varying thickness.
3. Use eddy current NDE methods to assess the minimum detectable flaw (size and/or depth) in each material system as a function of TPS thickness.
4. Assess potential areas where advanced development may enhance the limits of detection pertaining to RLV/TPS applications (probe design, advanced signal processing, etc).

This study was intended to provide an experimental assessment of the capabilities of eddy current methods in materials that closely represent those of suborbital RLV configurations. The intent was to study this NDE technique (eddy current inspection) on simulated RLV flaw standards in order to understand the technique's benefits and limitations and the potential for advances in its development to fulfill future needs of RLV developers. While improved quantitative understanding of detection limitations is provided through this effort, this work was not intended to be a rigorous probability of detection study for eddy current inspection.

The experimental approach used this evaluation followed a sequence of material preparation and evaluation that can be described under the following five subtasks: (1) selection and fabrication of candidate material systems, (2) flaw configurations induced in material coupons, (3) approach and application of eddy current inspection techniques, (4) results bounding the limits-of-detection using current state-of-the-art eddy current methods, and (5) potential direction of advanced developments in this field.

3.1 Selection and Fabrication of Candidate Material Systems

The selection of substrate materials for this study was based on the most probable types of material systems likely to be employed as structural skins on near-term, suborbital RLVs. The electromagnetic properties of a specific substrate material are important factors in the assessment of the eddy current flaw detection. However, given the scope and objectives of this study, the selection limited to one representative aluminum alloy, 6061-T6, and one composite material, graphite/epoxy. Specimens of each type of substrate material were obtained and cut to create test coupons approximately 4 in. x 4 in. by 1/8 in. thick. The coupon materials were visually inspected for surface defects and scanned using an eddy current probe to characterize their response prior to creation of simulated flaws. The methods for inducing systematic flaws will be discussed in another section.

The simulated thermal protection material selected for evaluation was a system of thin cork sheeting material (1/16-in. and 1/32-in. thick). Because typical TPSs range from a number of ablative or durable

thermally insulating, low-density material systems that may be bonded or sprayed onto the substrate, multilayer cork sheeting provides a convenient way of achieving TPS thickness variations. The intention in this study was to simulate the standoff (or lift-off) height of the eddy current inspection probe (coil) imposed by a generic TPS. As dielectric systems, most TPS materials, including cork, affect the electromagnetic interaction of the probe and substrate only by altering the probe proximity. This effect is easily simulated using an air gap, glass slide, or any number of nonconductive intervening materials. The selection of cork has the added benefit of providing an actual TPS-like surface texture relevant to the resolution limits for flaw detection. Application of the cork sheets to the substrate materials and the selection of TPS thicknesses used in the study are described in another section.

Figure 3-1 shows a photo of the selected substrates and TPS cork material used in the study.

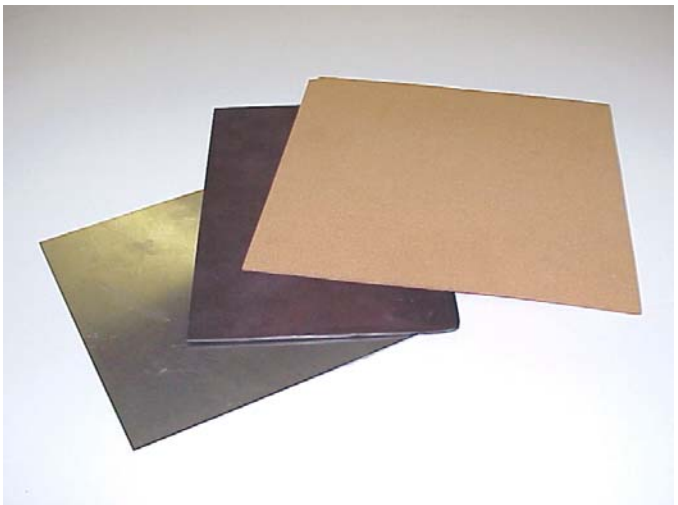

Figure 3-1. Substrates consisting of 6061-T6 Al plate and graphite/epoxy composite sheet; simulated TPS represented by thin cork sheet overlays of varying thickness.

3.2 Material Flaw Configurations

In order to assess flaw detection sensitivity as a function of TPS thickness, a range of simulated flaws or material damage was created in the substrate coupons. The typical flaw configurations found in metal alloy structures are likely to be small surface or subsurface cracks, possibly arising around welded joints or regions subjected to cyclic fatigue stress. The most prominent damage mode in graphic/epoxy composite structures is impact damage, which often results in the delamination of the internal layup structure, accompanied by a complex network of broken graphite fibers.

3.2.1 EDM Notches in Alloy Substrates

Creating and controlling the dimensions of a real crack in a material test coupon can be a formidable task. Generally, a fine crack can be induced and grown by subjecting a specimen to repeated, cyclic fatigue loading. A specimen is usually prepared with a machined notch that serves as a stress concentrator in the gauge region where the crack is desired. After the initiation and growth of the fatigue crack, the specimen surface is machined to eliminate the presence of the notch, leaving only the surface crack. A simpler, alternate approach is to create very fine notches by electronic discharge machining (EDM) methods. EDM

methods are often used to create pseudo-flaws for NDE evaluation standards because the process offers better dimensional control and is faster than real crack generation techniques. However, a machined notch, with specific width, may not always emulate the flaw response of a tightly closed crack. This has been an issue of some debate within the NDE community. Due to limitations of scope and budget, our approach was to substitute an array of EDM notches for real cracks. Since our principal objective was to determine the effects of TPS thickness on the limits of detection, the EDM notch served as a convenient benchmark, despite any differences in detection between the notch and real crack. As an accompanying effort, a comparison of the eddy current response produced by a notch with that produced by a real crack (in an available existing specimen from a separate study) was also evaluated to assess how the response signal may vary.

Two coupons of aluminum alloy substrate were processed with EDM notch features. Two notch depths were produced at two different notch lengths (two notches each on two 4 in. x 4 in. x 1/8 in. plates). All notch widths measured 0.020 in. Photographs of the EDM notch are shown in Figure 3-2.

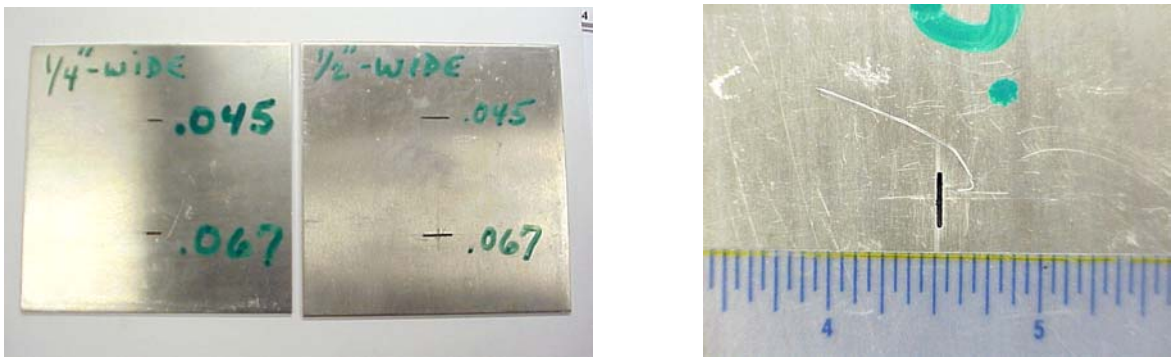

Figure 3-2. EDM notches produced on two 4 in. x 4 in. x 1/8 in. thick 6061-T6 aluminum plates.

3.2.2 Alternate Crack Fabrication Approaches

Alternate approaches to creating specimens with "fabricated" flaws were explored in an effort to achieve a "crack-like" feature that more closely resembles a real crack in contrast to an EDM notch. The goal was to obtain an eddy current detection response from the fabricated flaw that is as close as possible to the real crack response. In our first attempt, a flat plate specimen was cut in half, and the edge surfaces were polished smooth. The two halves of plate were then rejoined using an electrically conductive filler (silver loaded epoxy, tin-lead solder, indium thin foil, etc.) in all areas of the joint except for the defined crack feature. Figure 3-3 shows a schematic diagram of the sequence for creating the thin "crack-like" feature in the center of the flat plate. While the filled joint may indicate a degree of eddy current sensitivity when the bare surface is probed with the coil (i.e., its presences can be distinguished due to variation in electrical conductivity across the joint), its detectivity may drop rapidly after applying a thin layer of the TPS (cork). If the crack-like region is detectable for a given TPS thickness but the joint is not, the system would be viable for evaluating crack detection sensitivity as a function of TPS thickness.

This method was attempted first on a specimen of copper plate, rejoined using tin-lead (SnPb) solder on half the length of the plate. The results in this system were very successful in producing a bondline that responds like the parent material and an unbonded interface that resembles a very fine crack (0.002-in. maximum width) through the plate thickness. Figure 3-4 shows photos of the rejoined copper specimen

with a polished surface. The region containing the solder joint showed very little detection fluctuation in the eddy current response signal, while the "crack" region showed a considerable large detection signal. As a quick-look effort to see the effect of an overlay of cork, the crack was still detectable above 2 layers of 1/16-in. thick cork sheets. Further detail on the response of this copper specimen will be provided in a later section (3.5, Directions for Advanced Development).

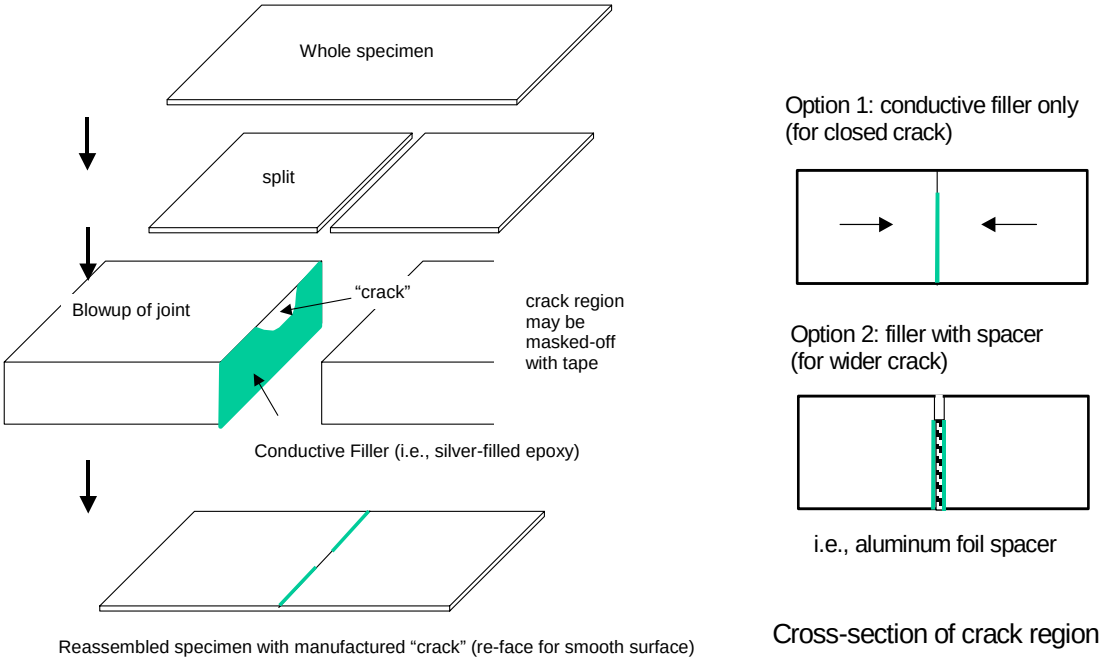

Figure 3-3. Sequence of steps to fabricate a closed "crack-like" flaw by a rejoining method.

Figure 3-4. Example of filled-joint technique for creating fine crack-like flaws for subsequent eddy current detection. This trial was made using a copper substrate and SnPb solder as the filler material (left). Crack detection was successful above 2 layers of 1/16-in. thick cork (right).

Unfortunately, while this re-joining effort showed promise on a specimen of copper, the eddy current detectivity of a similarly filled joint in 6061 Aluminum alloy was too high to provide good simulation of the an isolated crack (a finite length crack in the middle of a plate). The lack of success may be due the thin oxide layer which readily forms on the aluminum surface and limits the electrical conductivity at the joint interface. Such oxides do not form on copper, and thus, a high conductivity path across the re-joined Cu interface provides a sharp contrast to the non-joined "crack" region.

Our final attempt to fabricate a crack specimen involved a method whereby cracks of variable width but infinite length could be used to measure eddy current detection sensitivity with TPS thickness. Detection sensitivity to crack length can be scalable to the diameter to the probe tip (or effective diameter of the induced current), thus the results would be relevant to configurations of finite cracks with an appropriately-sized, small diameter pencil probe. Split-plate specimens of three different thicknesses were fabricated and assembled using a pliable silicone adhesive. The split-plates were bonded onto a Plexiglas base capturing a substrate of aluminum alloy under the split edges as shown below in Figure 3-5. The split-plate was bonded only to the Plexiglas base while maintaining "crack gap" of 0.020 inches, but outer edges of the specimen could be squeezed in a vise or clamp in order to vary the crack width. Ultimately, the split-plate can be compressed to form a completely closed "crack" with a depth equal to the thickness of the split-plate. Figure 3-6 shows photos of the one split-plate specimen in the fully open (0.020 wide crack) and closed condition (tightly closed crack).

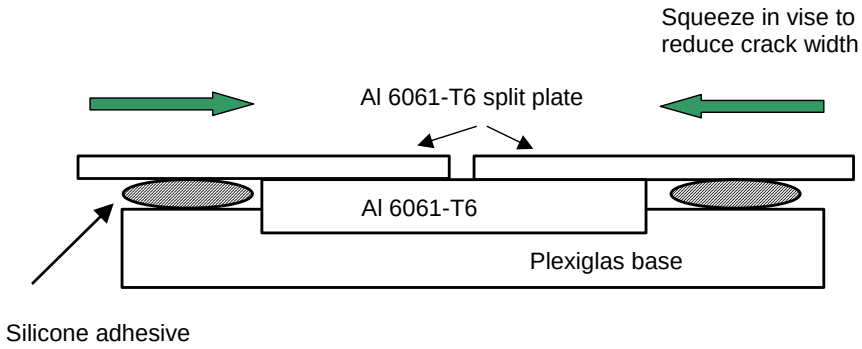

Figure 3-5. Schematic diagram of split-plate coupon with variable crack width. Coupons were made with an initial crack width of 0.020 inches. Silicone adhesive allows plates to be compressed in a vise to achieve a completely closed crack.

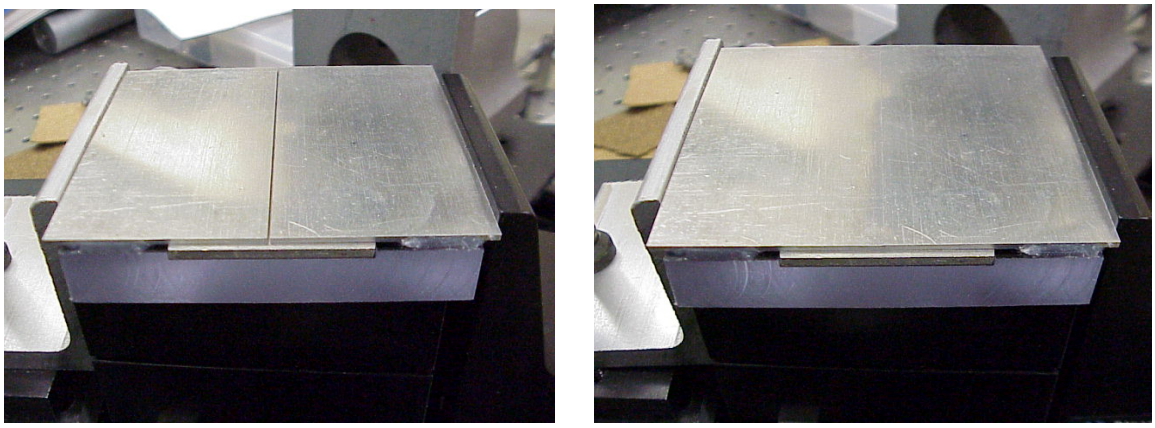

Figure 3-6. Example of split-plate coupon in test set-up vise prior to eddy current inspection measurement. Left, fully open crack (0.020-in.), right, completely closed crack.

Initial measurements using the variable split-plate coupons indicated that the detection response in the closed condition is very similar to that anticipated for actual tight, fatigue cracks in metals. Thus, variable split-plate coupons in crack depths of 0.090, 0.048, and 0.018 inches (thickness of thin plate stock of 6061-T6) and width openings of 0.020, 0.010, and zero width, were adopted for the detection matrix of this study (Figure 3-7). Crack length will not be a parameter in the study, however the results should be relevant to situation where optimum detection sensitivity is achieved using a small tipped probe for finite length cracks.

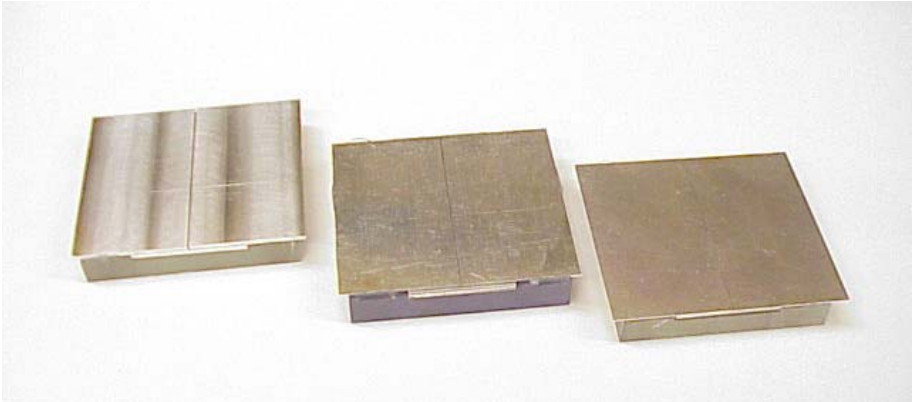

Figure 3-7. Variable split-plate coupons representing three different surface crack depths. The thickness of the upper plates (0.090, 0.048, 0.018-in.) define the crack depth.

3.2.3 Impact Damage in G/E Composite Substrates

Initially, two pathfinder composite coupons were subjected to impact loading events in order to bracket the range of loading required to induce delamination/broken fiber-type damage appropriate for subsequent eddy current detection. Our in-house, instrumented impact-testing machine (Instron Dynatup) provided characteristic load/energy/deflection data for each impact and allowed a careful assessment of the graduated

impacts necessary to induce various amounts of composite damage. Our goal was to impact the first composite specimen at a level that produced only slightly detectable damage when inspected by eddy current at the bare surface. It was expected that with the smallest increment of probe lift-off (thinnest TPS layer), the flaw damage would be below the detection threshold. With increasing impact energy, the degree of damage would be greater (larger area and higher number of delaminations and broken fibers) and the flaw detectability would be measurable with increasing TPS thickness. There would, however, be some limit in TPS thickness beyond which no detection capability exists regardless of the magnitude of damage.

The impact testing system is shown in Figure 3-8. Figure 3-9 shows a view of the composite specimen support apparatus within the impact testing rig. The first specimen was restrained with mounting clamps at two opposite ends and was subjected to a 120 in-lb energy impact using a 1.5-in. diameter tup. The resulting damage zone was quite visible from both front and rear surfaces. Specimen 2 was installed using a "picture-frame" mounting arrangement (stiffer configuration) and was subjected to a 30 in-lb impact with no visible damage detected. A handheld eddy current scan was made across the impact zone, and no damage response was observed. Several additional impacts were performed at increasing energies until some detectible damage was observed on the surface. From these trial experiments, five impact levels (45.4, 68.0, 79.4, 90.7, and 136.1 in-lbs) were selected for the five composite coupon used in this study.

Figure 3-8. Instrumented impact testing machine used to create flaws in composite specimens.

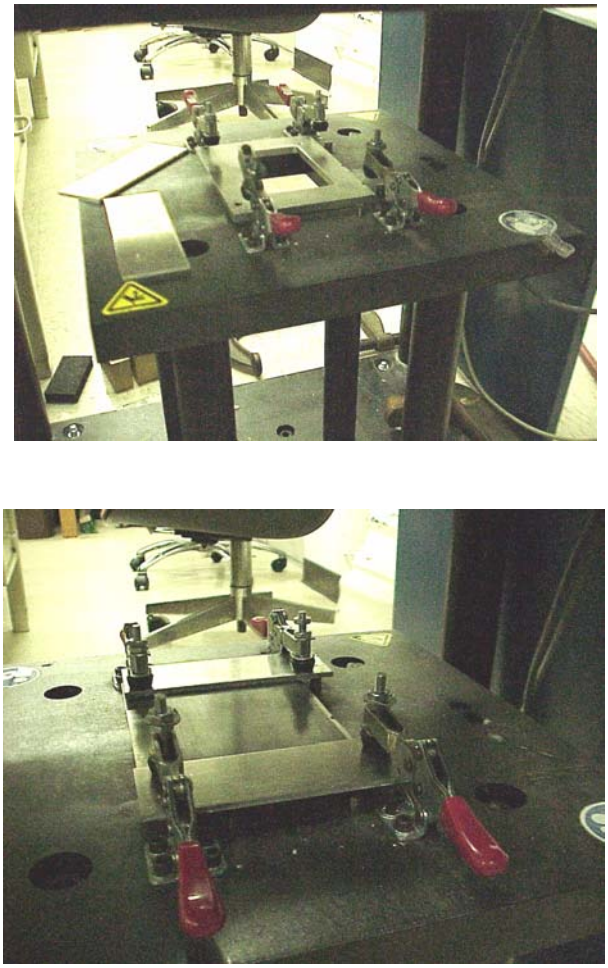

Figure 3-9. View of composite specimen support apparatus within impact testing rig.

Figure 3-10 shows photos of the front and rear surfaces of the composite coupons after sustaining impact damage. The dimensions of the individual graphite epoxy composite coupons, 4” x 6”, was based on the existing support hardware used in the impact testing fixture.

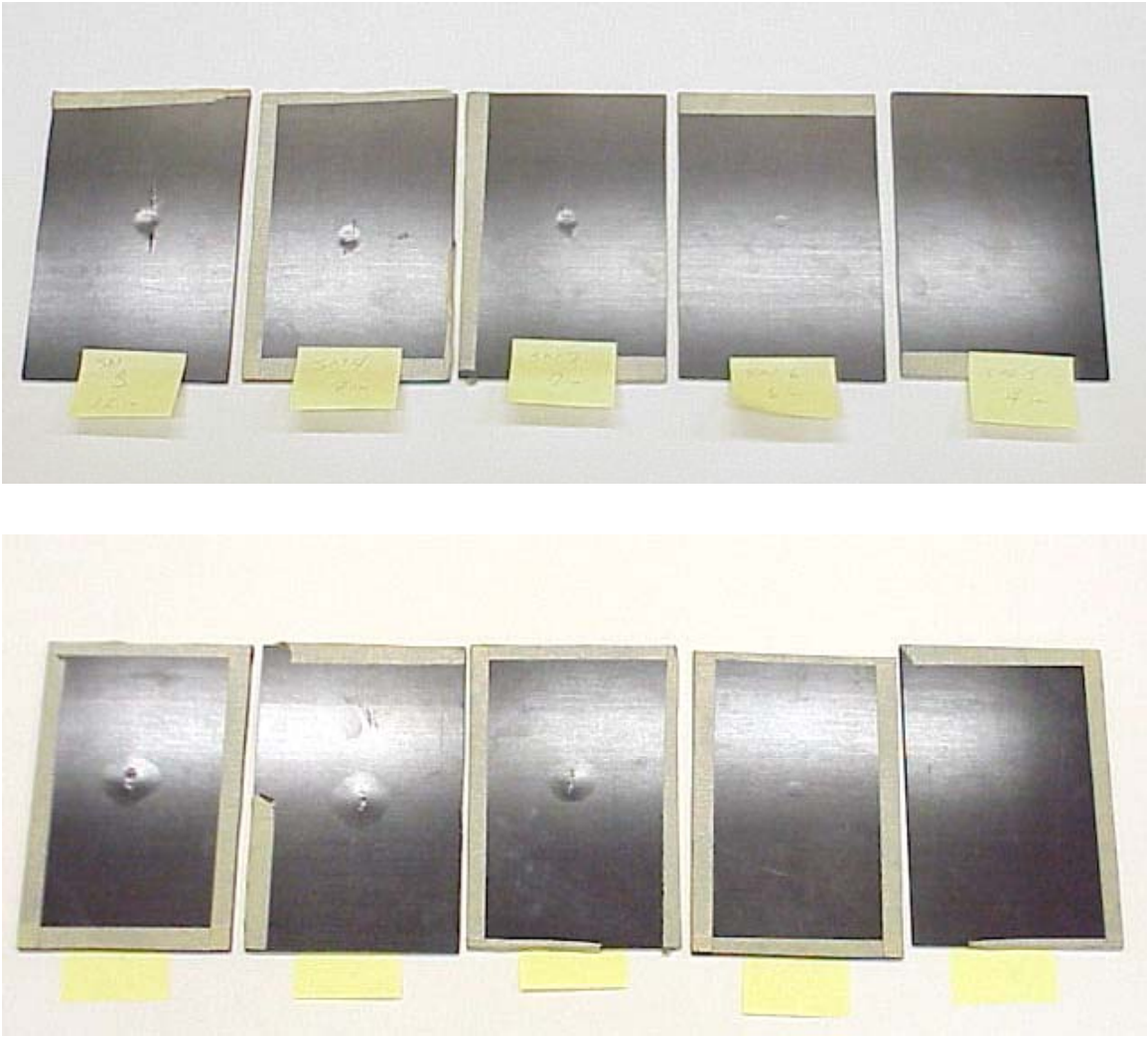

Figure 3-10. Front and rear surfaces of composite specimens with impact damage. Impact energies (from left) 136.1, 90.7, 79.4, 68.0, 45.4 in-lbs. Note: no discernable damage at lowest level impact; distinct damage threshold between 68.0 and 79.4 in-lbs; small change in magnitude of damage from 79.4 to 136.1 in-lbs.

The higher levels of impact energies resulted in a progression of damage characterized by a distinct depression on the impact surface (front) and a blister on the opposite surface (rear), presumably the result of delaminated plys throughout the thickness of the composite (originally 1/8” thick). Accompanying the delamination damage were visible cracks on both surfaces running primarily with the long axis of the coupons. Unfortunately, no information about the layup design or material

properties are available for the G/E composite used in this study. No efforts were made to rigorously characterize the extent of damage by alternate NDE methods other that to use infrared flash thermography to image the internal delamination zone in each coupon. Figure 3-11 illustrates an example of the thermography results. The thermographic images highlight detail regarding the extent and shape of the delamination damage. Near surface as well as deeper ply separation damage can be revealed which would not otherwise be evident by visual examination. The threshold for distinct visual damage occurs between 68.0 and 79.4 in-lbs. Slight indication of delamination was discernable at 68.0 in-lbs with thermography. Above 79.4 in-lbs, the increase in delamination area is only slightly measurable. A subtle progression in damage is noted primarily by an increase in length of the induced surface cracks with increasing impact energy.

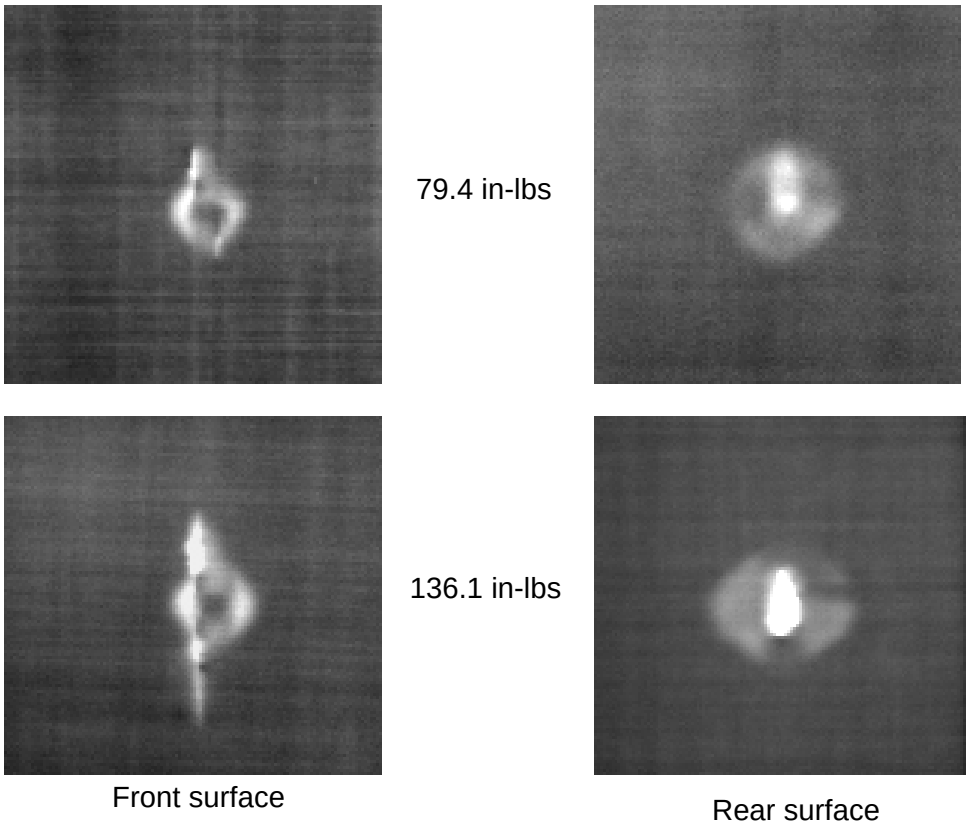

Figure 3-11. Images obtained with infrared flash thermography showing indications of the extent of internal delaminations (light areas) in two of the impacted composite specimens.

3.3 Approach and Application of Eddy Current Inspection Technique

Conventional methods for in-field eddy current inspection typically involve instrumentation similar to that shown in Figure 3-12. A variety of coils designs or probes is also shown in the figure on the right. Probe selection may be based on coil configuration (single, multiple reflectance-type, etc.), response frequency, and target geometry (flat, curved, cylindrical surface). Figure 3-13 illustrates a

flat, hand-scan configuration initial proposed for the TPS-covered substrate crack detection in this study. Important aspects of probe design parameters will be discussed in a later section.

Figure 3-12. Portable eddy current test unit (Zetec MIZ-22) typical of common field instruments optimized for a variety of inspection applications. Typical variety of search coil probes used on flat targets.

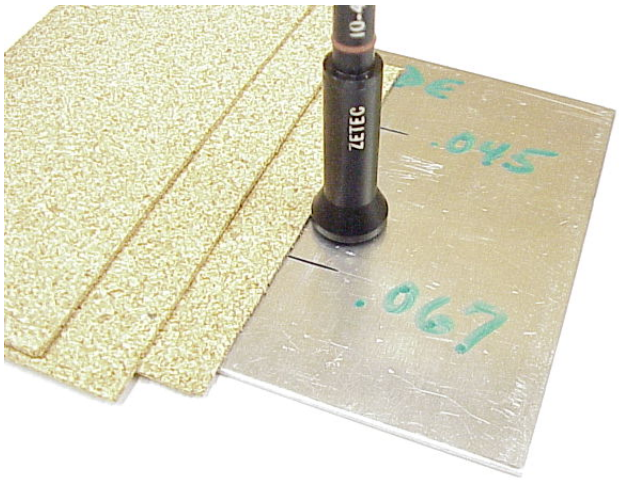

Figure 3-13. Example of inspection setup for detection of defects on bare substrate and with incremental TPS thickness (multiple cork sheets).

Flaw detection is signified by a change in coil impedance as the probe is positioned, or slowly scanned, across the flaw region. The impedance change is typically presented in most modern inspection units as a deviation, or the trace of the locus of points in an X-Y phasor display of the phase and amplitude of the complex impedance (as illustrated earlier in Figure 2.5). The limit of flaw detection is reached when the presence of the flaw no longer causes a recognizable deflection trace on the screen display. Often, at the highest gain setting available on the detection unit, the trace

point becomes a noise disk. Contributions to the loss of resolution are also due to signal jitter caused by probe tilt and surface texture causing vertical motion. Figure 3-14 shows a schematic and actual data of the complex impedance change for a real fatigue crack (in a Ti-6Al-4V fatigue specimen), scanned at the surface (zero lift-off), plotted as the real (resistance) and complex (inductive reactance) impedance components in the X-Y display of the eddy current testing unit of Figure 3-12.

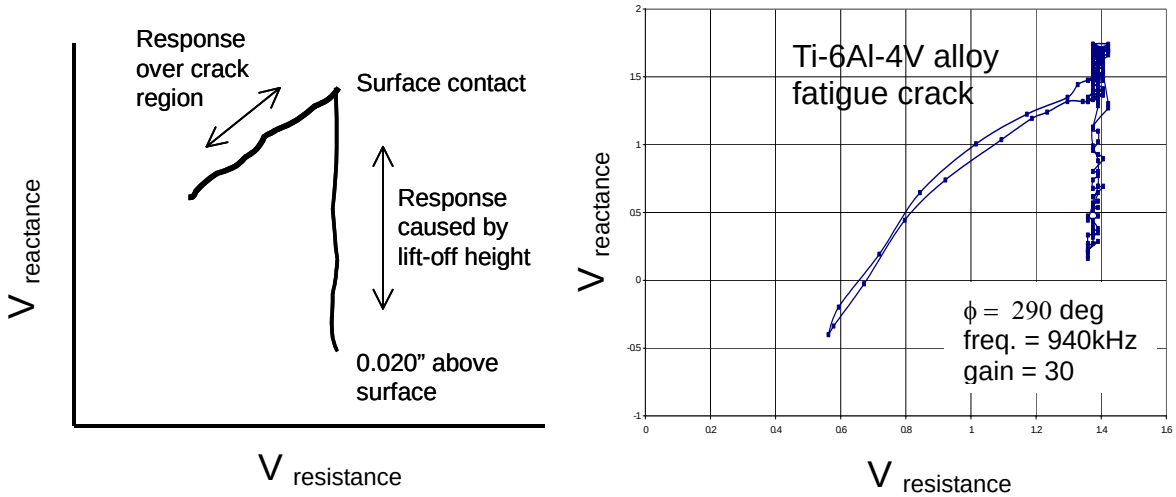

Figure 3-14. Schematic and actual data obtain from an eddy current probe scan over a closed crack in a fatigue specimen of Ti-6Al-4V. The plots show the trace of the impedance change produced by the presence of the crack as well as the effect of slight probe lift-off. Note: units scaling in all impedance plots is abritrary.

It should be noted that the test parameters identified on the data plot include: phase angle Φ, which essentially aligns the rotational orientation of the display (our set-up orients pure resistive change along the horizontal axis); coil excitation frequency, which relates to skin-depth or crack depth resolution. Test frequency was adjusted to probe near the resonance frequency of each coil/target configuration for maximum sensitivity (the rationale for this will be further developed in Section 3.5). Finally, the gain setting for the display is noted which can be important for target response comparisons.

For the set-up conditions under which this target was measured (as well as the bulk of all measurements made in this study), some fundamental observations about the eddy current signal response (impedance change) should be illustrated before proceeding to the TPS matrix measurements. With the aid of a conductivity calibration standard, the relative impedance change due solely to the effect of material conductivity may be plotted and then superimposed on any flaw or crack response. Figure 3-15 shows a simple conductivity standard made of coupons of Cu, Al, Brass, and Nickel, and the response when a probe is sequentially placed over each of the coupons. The dotted line over the conductivity response represents the path of the inductance change for small changes in electrical conductivity. On first order, a tightly closed crack (with no air gap) should affect the induced eddy currents as if the material conductivity was slightly altered at the crack plane. Thus, the response for a tightly closed crack should follow this path line. This is demonstrated for the fatigue crack in Ti-6Al-4V as the eddy current response follows the conductivity path between the

titanium alloy and a graphite conductivity specimen in Figure 3-12 (continuation but different scale range than Figure 3-15).

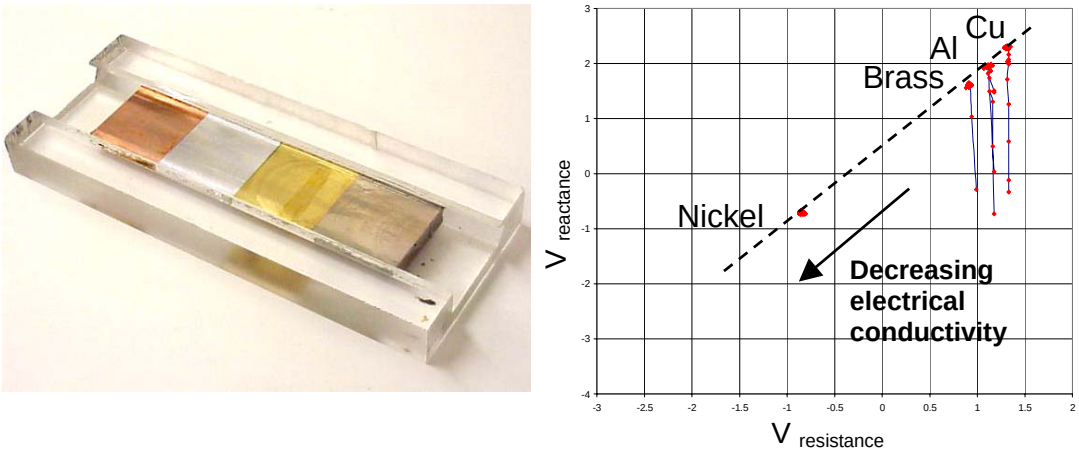

Figure 3-15. Photo of metal conductivity standard and results of coil/target impedance change measured with the eddy current probe at the surface of each metal.

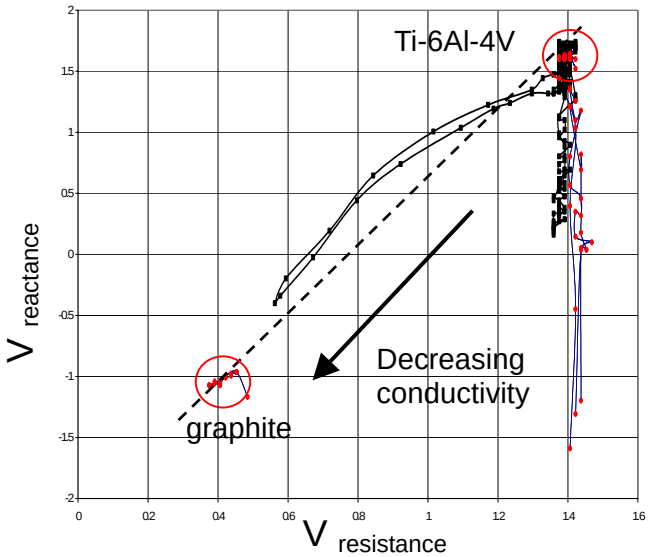

Figure 3-16. Eddy current response for closed fatigue crack in Ti-6Al-4V follows the conductivity path between the titanium alloy and a graphite (lower conductivity) specimen.

It will be shown below that the 6061-T6 split-plate specimens simulate a closed crack in aluminum very well by this criteria (unfortunately, no real fatigue cracks in this alloy were available as a direct comparison for this study).

Another observation regarding the observed impedance response concerns the relationship of the lift-off response signal to the flaw response. For our set-up conditions, we have adjusted the testing

frequency to remain at the coil/target resonance frequency (varies with material and lift-off height) for maximum sensitivity of response. Because the phase angle of the unit display can be arbitrarily adjusted to any angular orientation, a pure resistive change is assigned to the horizontal axis (determined with a pure resistive load). Thus, the resonance frequency can be experimentally determined by seeking the frequency that aligned the lift-off response with the vertical axis (i.e., zero resistance at the resonance). The significance of the lift-off response is that it identifies the direction for the impedance change path as a crack increases in width. In other words, as the crack opening increases (wider crack) the eddy current response displays components of both the conductivity change (closed crack) and the effect of lift-off across the crack gap, thus, a change in slope toward the pure lift-off path line. This is schematically illustrated below in Figure 3-17.

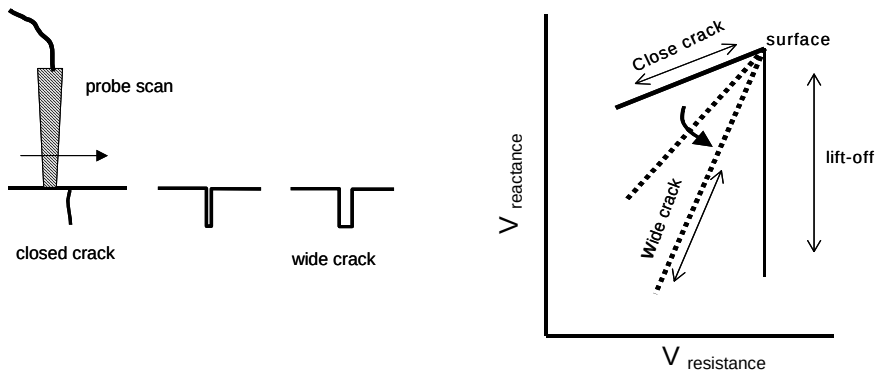

Figure 3-17. Change in eddy current response signal as probe is scanned over a tightly closed crack verses cracks with of equal depth but greater width.

Note that, for wider cracks, as the slope approaches the pure lift-off orientation, the magnitude (length) of the signal increases, or alternatively, the magnitude due to the conductive component is unchanged. It is typical of most inspections that optimum set-up conditions (operating frequency, etc.) allow for a distinction between flaw detection and lift-off effect. This is because manual inspection scans are often difficult to achieve without extraneous lift-off effects caused by surface roughness or vibration. This sensitivity to vertical displacement was encountered as our initial measurements were made over the soft cork material intended as the TPS model for this study. Slight variations in probe pressure caused signal lift-off "noise" that made flaw signal recognition difficult at high gain settings. Although such limitations are pertinent to this study (but limited to soft-surfaced TPS), a more systematic approach for the effects of TPS thickness was adopted by supporting the probe at a calibrated height above the target (within a scanning fixture). Figure 3-18 shows the inspection configuration ultimately used in this study.

The effects of crack depth on the signal response is illustrated by the results obtain with measurements made using a grooved inspection standard. A aluminum standard fabricated with 0.005-inch wide grooves with depths of 0.008, 0.020, and 0.040 inches was inspected using the same coil and set-up conditions as in the prior measurements (at resonant frequency, same phase, gain, etc). The effect of a systematic increase in flaw depth is to increase the magnitude of the response signal while preserving the orientation of the impedance change path line with respect to pure lift-off. This is illustrated below in Figure 3-19.

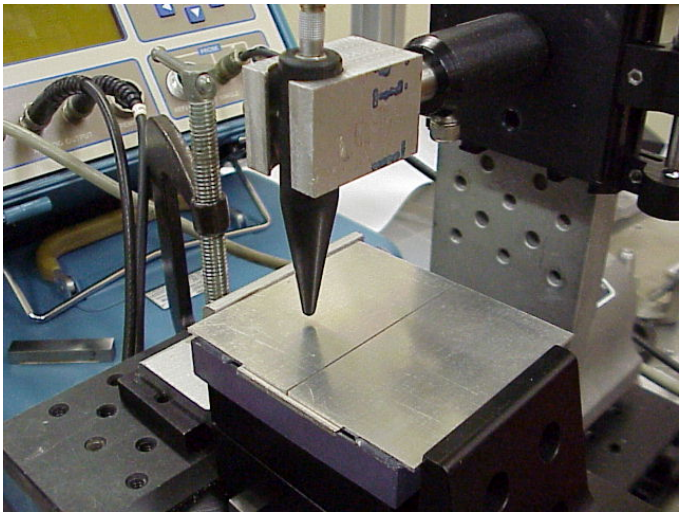

Figure 3-18. Eddy current inspection set-up. Support structure for probe on micrometer control stage to adjust probe height (TPS thickness). Split-plate coupon, held within vise to adjust crack width opening, mounted on scanning translation stage.

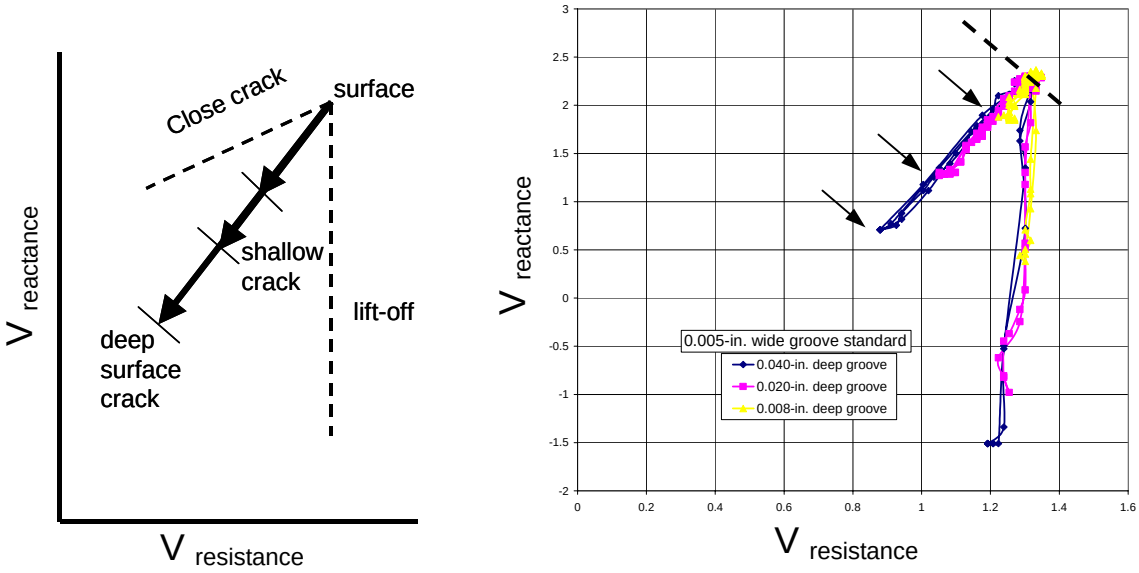

Figure 3-19. Schematic and actual data obtain from inspection standard of equal width grooves of varying depths.

3.4 Results Obtained for Limits of Detection with TPS Thickness

The utility of the 6061-T6 aluminum variable split-plate was demonstrated by how effectively the three coupons (with different crack depths) exhibited the impedance response trend described above. Each coupon was scanned at the surface using the same eddy current probe while the clamp fixture allowed the crack width to vary from completely closed to a maximum width of 0.020 inches. An example of the response in shown in Figure 3-20 at three specific widths for the coupon with a 0.090-in. depth crack. The data show that the closed-crack response is very close in slope to the conductivity path line obtained using the conductivity standard (partial data is also superimposed). The split-plate coupons, however, did exhibit some anomalous behavior in their simulation of real cracks. The trend of increasing signal response with increasing crack depth demonstrated with the grooved standard was not consistently displayed by the split-plates. One reason may be that as the thin split-plates are forced together, some separation with the base material can occur, causing the change in "sub-surface" structure to contribute to the signal response. This is illustrated in Figure 3-21. Future enhancements, beyond the scope of this current study, will involve maintaining downward pressure on the split-plate, and using a base material of higher conductivity (such as copper) to further inhibit the "sensing" of the base-plate/split-plate interface.

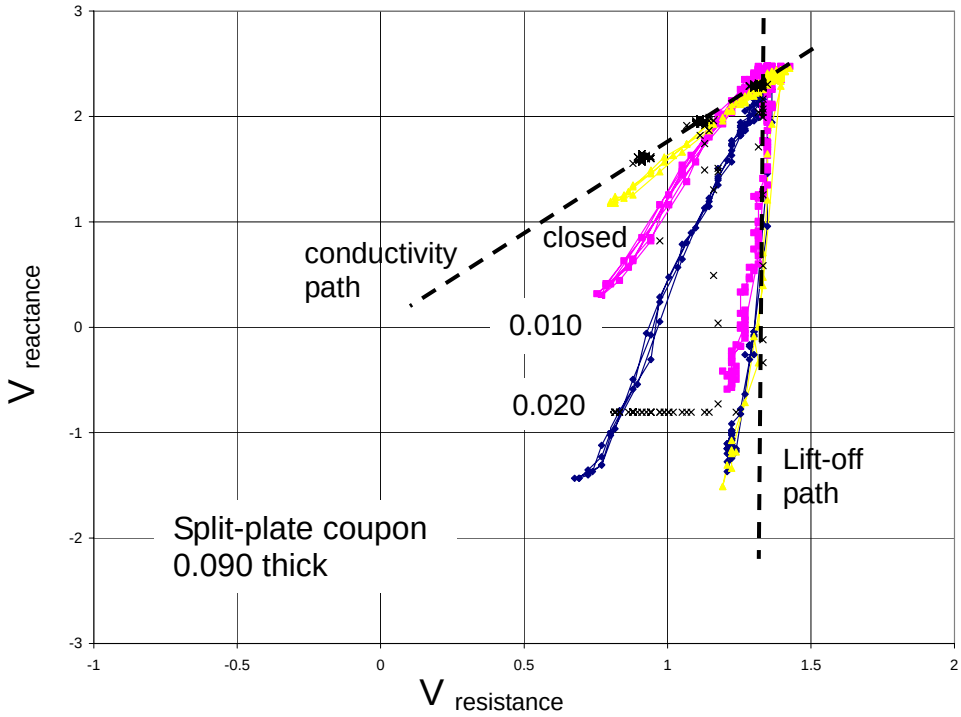

Figure 3-20. Schematic and actual data obtain from inspection standard of equal width grooves of varying depths.

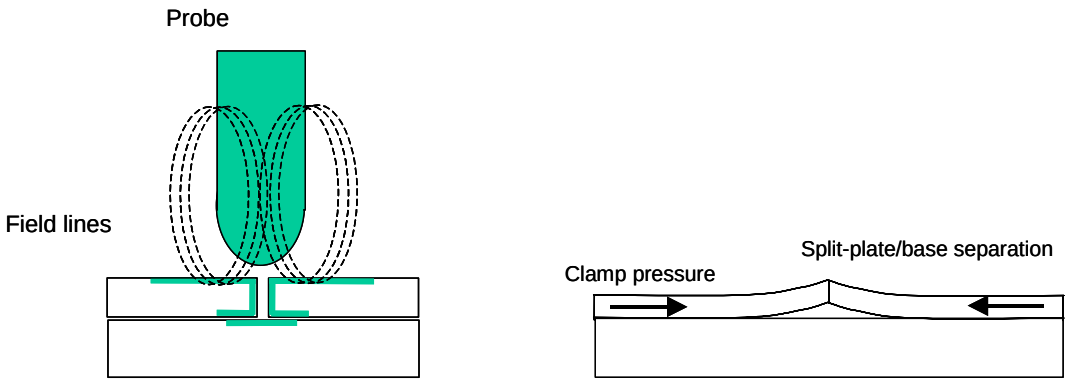

Figure 3-21. Issues identified which may cause spit-plate coupon response to deviate from a real surface crack. Left, base/split-plate interface contributes to response signal; right, thin plates (shallow cracks) deflect upwards with clamp pressure.

Although the present design of the coupons exhibited some departure from expected behavior, it was felt that the change in the relative sensitivity of flaw detection with TPS thickness could still be viable for a test matrix of crack depths and widths achieved with the split-plates. The crack matrix used in the lift-off sensitivity measurements included surface crack depths of 0.018, 0.048, and 0.090 inches, each at widths of zero, 0.010, and 0.020 inches. For each crack size, the eddy current response was recorded at probe heights of zero (at the surface), 0.04, 0.08, and .120 inches above the surface. The reduction in signal magnitude with probe lift-off distance was then calculated as a percentage of the maximum signal obtained at the surface. An example of the lift-off sensitivity data for the 0.018-in deep, closed crack (zero width) is shown below in Figure 3-22.

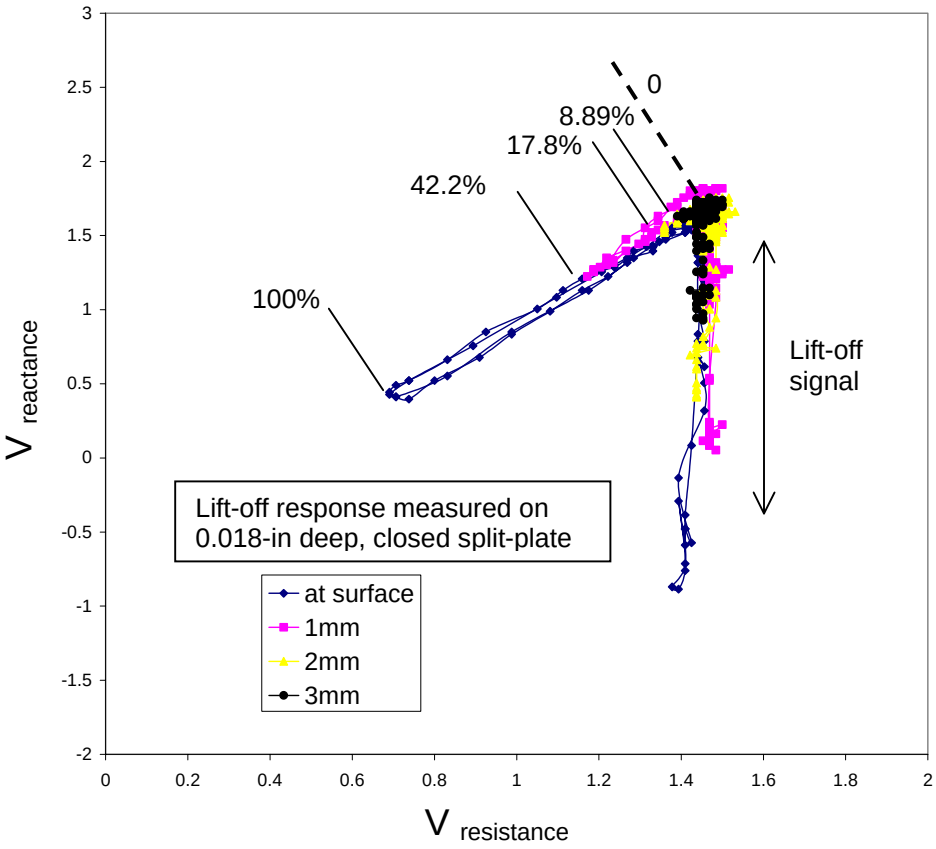

Figure 3-22. Variation in signal magnitude with probe lift-off distance for 0.018-in deep, closed surface crack. The change in signal strength shows the relative affect of increasing TPS thickness.

Similar measurements were performed on the EDM manufactured crack specimens. A comparison of the impedance response for the two notch depths is shown in Figure 3-23. As discussed above, the EDM notch response exhibits a greater slope than the closed cracks due to the width of the flaws. The deeper notch provided the greater signal as in the case of the groove standard shown earlier. When a split-plate was adjusted to nearly the same crack opening and depth as the EDM notch a stronger eddy current response was obtained, further confirming that the current split-plate design provides some impedance contribution from the base material interface. There was little change in signal when EDM notch lengths of 0.25 and 0.50 inches were compared, owing to the small diameter probe used in all of these measurements. Thus, the finite length notches may be appropriately compared with the infinite split-plate cracks. An example of the signal variation with lift-off is shown in Figure 3-24 for the 0.067-in deep, 0.025 wide EDM notch. Note that the sensitivity to lift-off is similar to the split-plate results. It should also be noted that as the signal level decreases with lift-off exceeding 0.120 inches (3mm), the response become difficult to resolve within the “noise disk” typical for most of these measurements (further increases in instrument gain will not improve signal resolution).

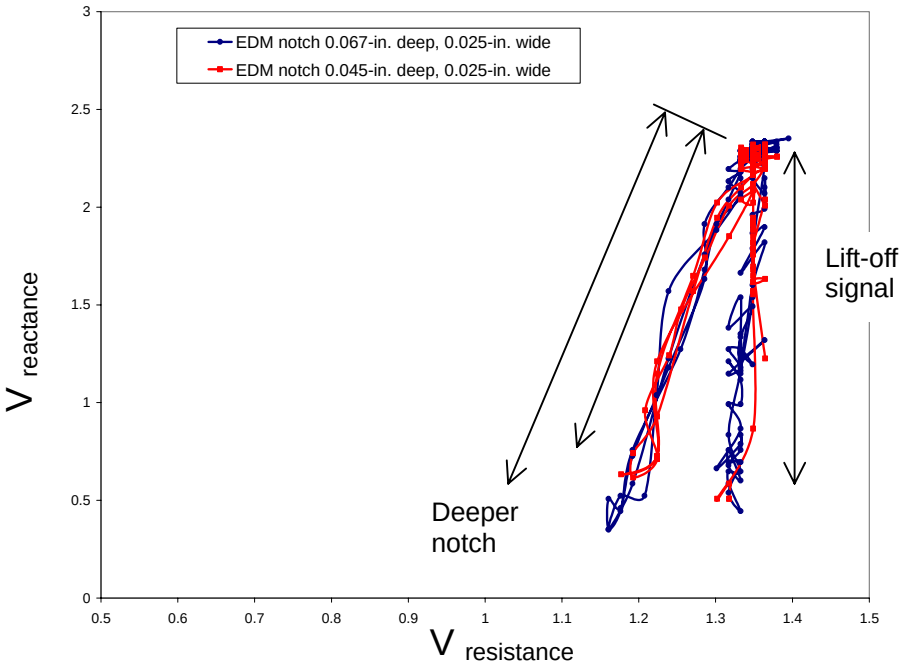

Figure 3-23. Results comparing the response of the EDM notches at two different depths, 0.045-in and 0.067-in deep. Both notches are 0.025-in. wide. For both specimens the notch length was 0.25 inches. Similar results were obtained for notches of 0.50 length due to the small diameter pencil probe used in the measurements.

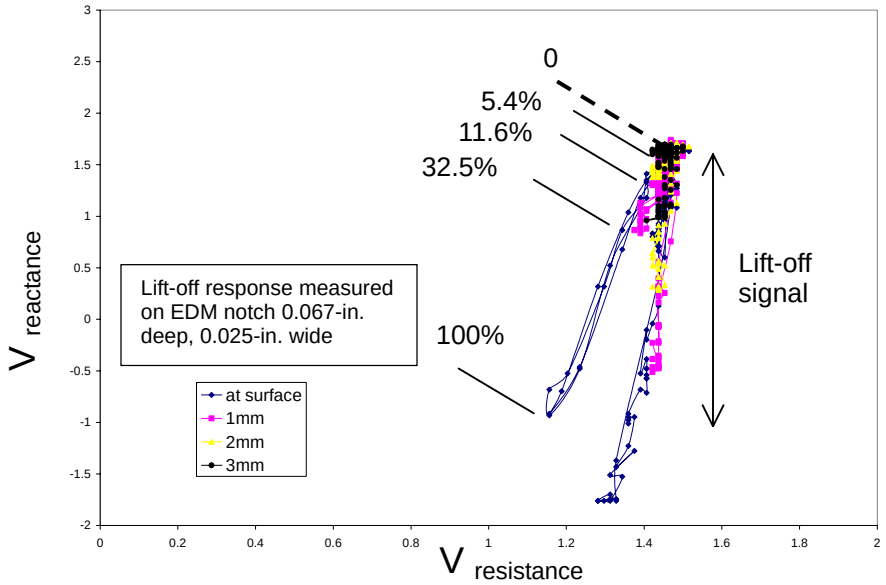

Figure 3-24. Variation in signal magnitude with probe lift-off distance for EDM notch 0.067-in deep, 0.025 wide. The change in signal strength shows the relative affect of increasing TPS thickness.

A summary plot of the data obtained with the 6061-T6 aluminum split-plate coupons and the EDM notch specimens to assess the sensitivity of the eddy current response as a function of lift-off height is presented in Figure 3-25. The results indicate that the effect of TPS thickness, when measured in proportion to the eddy current response at the bare surface, is virtually the same over the range of surface flaw configurations used in this study. The results show a 30-40% reduction in signal at a TPS thickness of 0.04 inches, 10-18% reduction at 0.08 inches of TPS, and for TPS thicknesses greater than 0.120 inches, conventional eddy current inspection will become very difficult due to poor flaw signal resolution.

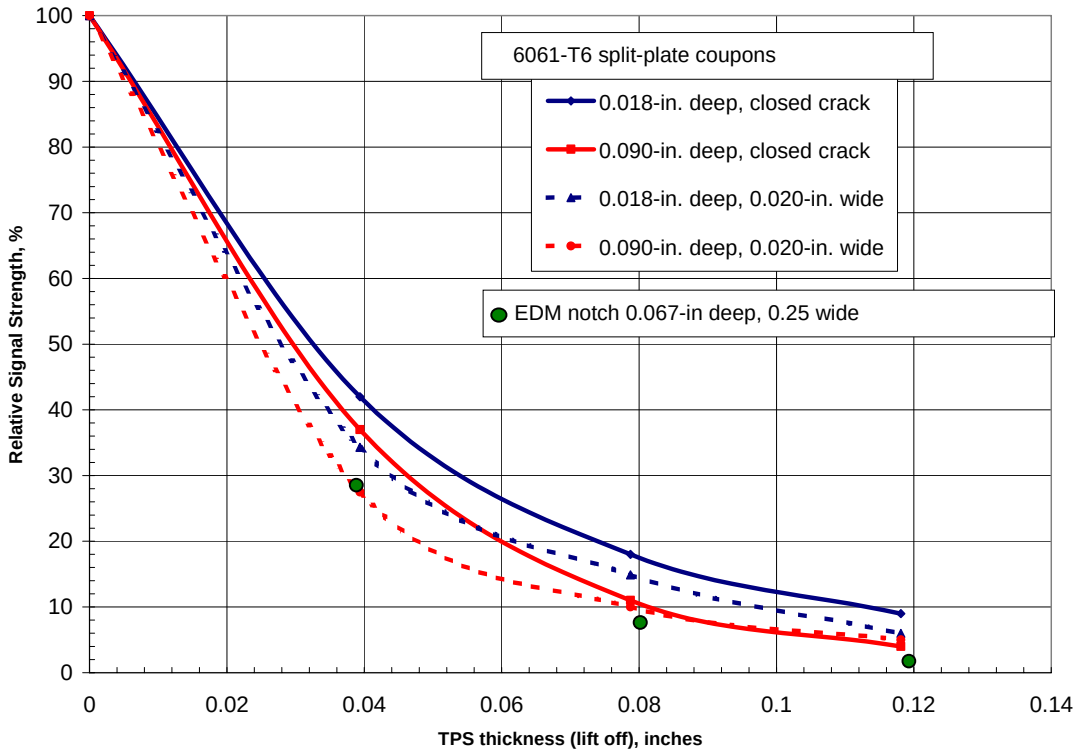

Figure 3-25. Results of lift-off sensitivity measurements. Magnitude of eddy current signal response with probe lift-off height shown as a percentage of signal obtain at surface (zero lift-off).

Noteworthy is that, while a matrix of crack configurations was evaluated in this study, the eddy current response due to depth and width variations is relatively minor compared to the much larger signal attenuation caused by probe lift-off. The graph indicates that closed cracks may attenuate in signal with TPS thickness only slightly less than wider cracks. In absolute terms, shallow surface flaws produce less impedance change than deep flaws, which make deeper surface cracks more easily detectible. However, rather than attempting to identify an absolute flaw-size limit for detectibility (which necessitates rigorous probability-of-detection methodologies with an abundance of control flaws and inspectors), the results of Figure 3-20 provide some insight for “scaling” a given surface inspection capability to an inspection with a specific TPS thickness. For the crack parameters chosen for this study, based upon the response obtained with the split-plate and EDM notch samples, crack detectiblity was found to fall just outside our instrument noise band at a lift-off height of 0.12 inches.

3.4.1 Results of Limits of Detection for Composite Specimens

Similar eddy current measurements were made on the impacted graphite epoxy coupons using the same probe and set-up approach described above for the aluminum alloy specimens. The undamaged regions of the impacted specimens displayed the same characteristic response as a control, non-impacted specimen. Scans were made just above the composite surface at a height necessary to avoid contact with the blistered surface of the most heavily delaminated coupons. A typical scan at the surface of an undamaged region is shown below in Figure 3-26 on the left. On the right is a trace showing the response due to probe lift-off. As described previously, the resonant frequency at the target/probe configuration was selected for maximum impedance response sensitivity, and is defined by the vertical lift-off orientation.

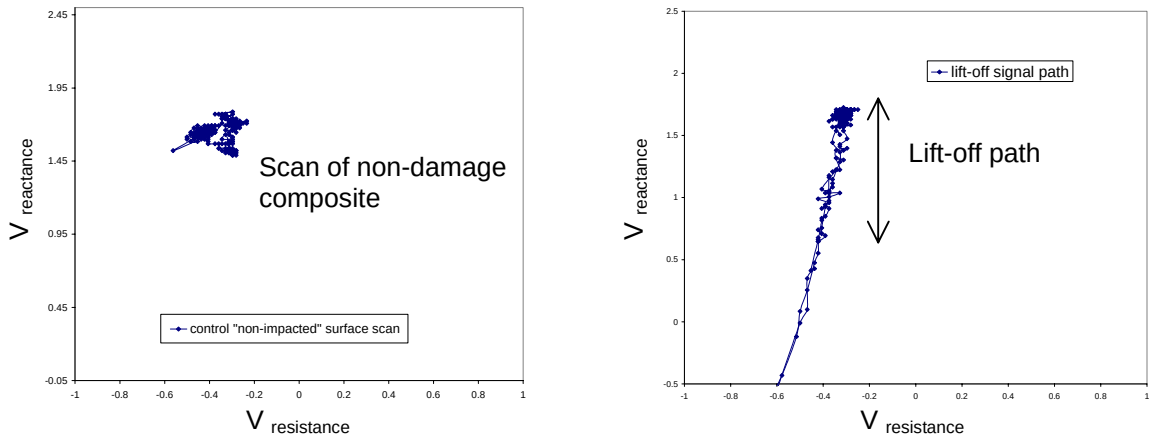

Figure 3-26. Results of scan on undamaged composite (left) and the response due to probe lift-off.

As contrast to this, an example of the resulting scan made on the most heavily impacted coupon is shown in Figure 3-27. The two orthogonal scans were made in the length and width directions of

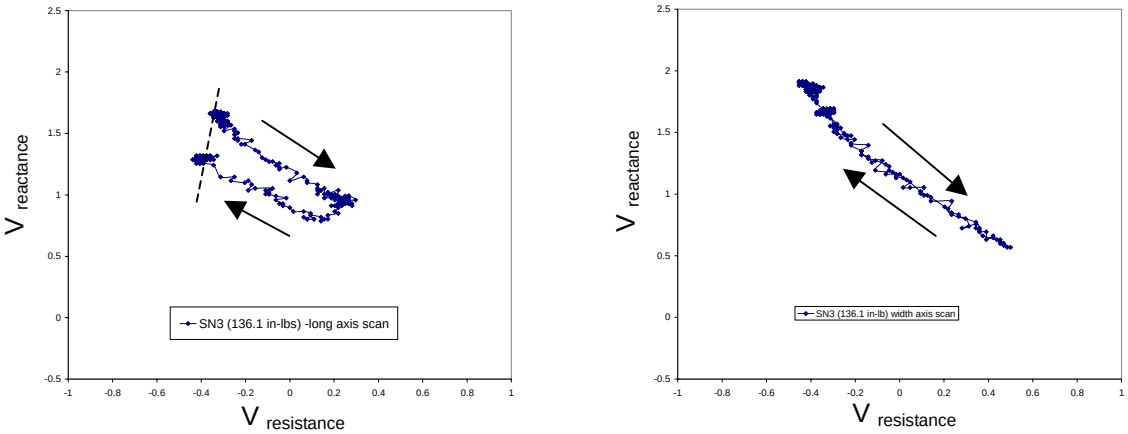

Figure 3-27. Results of two orthogonal surface scans on most heavily impacted composite specimen. Some surface tilt indicated as a change in lift-off distance from scan start to finish point.

the coupon. Some amount of surface tilt gave rise to the probe displacement shown in the plot on the left. The difference in signal change magnitude between the length and width scans may be due to the non-symmetrical extent of the delamination damage. The impedance change path observed for the composite damage is not as easily characterized as in the case of the crack geometry in the alloy system. It was noted that the greatest signal change was obtained when the specimens were scanned on the front (impacted) surface. This may indicate greater sensitivity of response due to compressed plys (visible surface indention) versus ply separation (blistered surface of rear face). No significant difference in response signature was noted when the probe was scanned directly over the visible surface cracks where broken fiber damage has occurred. It may be that the specific orientation of the broken fibers represents a small contribution to the entire volume of "material damage" sampled by pencil probe.

Scans were made at sequentially greater lift-off distances on each of the coupons. An example of the response at the surface of the most heavily impacted sample was shown above in Figure 3-27 (zero lift-off). Figure 3-28 shows how the response attenuates as the lift-off (representing TPS thickness) increase to 0.08 and 0.12 inches, which becomes the limiting regime for adequate signal recognition.

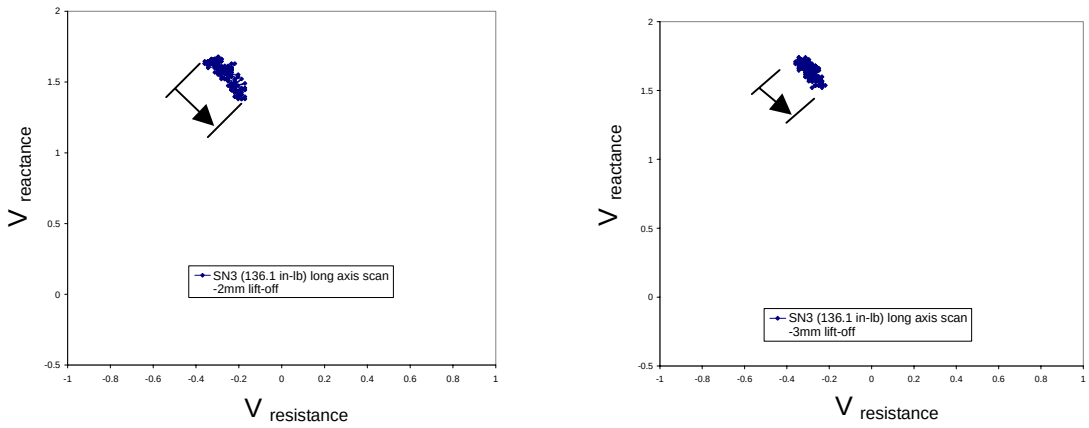

Figure 3-28. Attenuation in signal with probe lift-off increase from 0.08 inches to 0.12 inches on the most heavily impacted specimen.

In contrast to this, the result of scans made on the coupon which showed barely discernable damage (68.0 in-lb) at lift-off distances of zero (surface) and 0.4 inches are shown in Figure 3-29 on the next page.

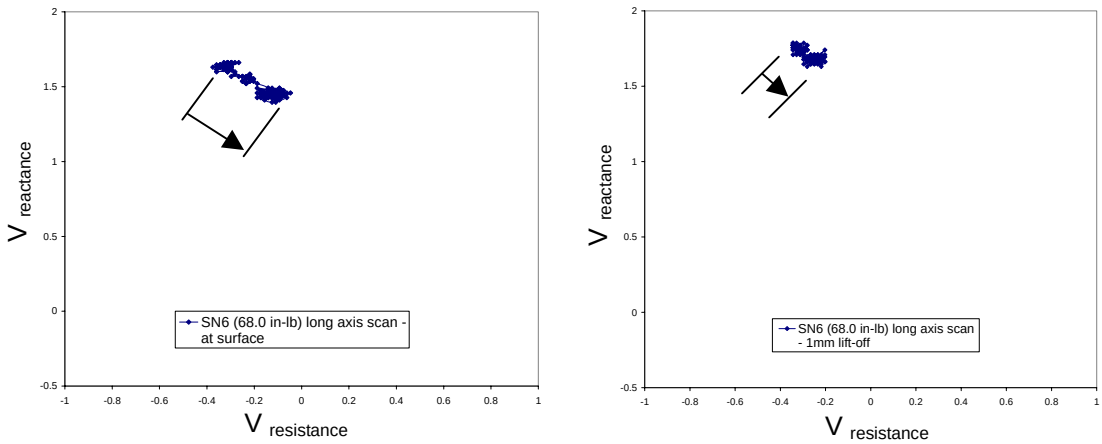

Figure 3-29. Attenuation in signal with probe lift-off increase from zero inches (surface) to 0.04 inches on the specimen which showed barely discernable damage (68.0 in-lb).

The results of the inspections perform on the impacted G/E composite coupons showed that conventional eddy current response at the surface (i.e. no TPS) could distinguish damage produced at a threshold level of impact which results in no visible damage, although some indication is evident by thermographic inspection. However, this response is only resolvable to a lift-off distance just above 0.04 inches. For higher levels of impact damage that results in clearly evident surface cracking and internal delamination, the eddy current response can be measured at lift-off of at least 0.120 inches, however at greater distances the damage response would be difficult to resolve.

3.5 Directions for Advanced Development

In an eddy current inspection, using conventional testing units like the one described earlier, the complex impedance (z_r and z_i) of a coil at a fixed frequency is monitored via the impedance plane diagram (z_r, z_i). The signal, however, is so highly dependent on coil design and operational frequency that it is often difficult to give clear meaning to a measured value or to directly compare measurements for two inspection setups. Therefore, standard practice is generally to look for relative local changes in the signal response over a specimen surface (under fixed instrument settings) to detect flaws. Such limitations are rooted in the fact that the measured complex impedance signal contains a mixture of external effects (coil, cable, and instruments) together with the response of the sample. In other words, a blind measurement (without a mechanism for isolating the sample's response alone) of the complex impedance at an arbitrary selected frequency cannot provide absolute information about the condition of a sample (specific flaw response). An alternate approach, however, for analyzing the impedance change, which borrows directly from methods used in microwave interaction studies, can be exploited to provide useful, specific information about the sample condition.

Our present investigation of eddy current methods and signal analysis has advanced under a closely allied, but independent, internal research effort aimed at developing electromagnetic techniques specifically for material properties evaluation. Early results of this analysis may be leveraged as a useful predictive tool that will aid and hopefully confirm the detection sensitivity matrix measured under this task.

The experimental setup for measuring the coil/material system impedance differs from that of the conventional eddy current unit used for the results describe above primarily in that the coil is continually driven at a swept frequency (tone burst). The resulting measurements revealed that the frequency dependent impedance behaves as a resonance with a maximum impedance at a well defined frequency. This resonance behavior can be understood by accounting for the capacitive elements represented by the cabling and instrumentation. The laboratory instrumentation setup used for these measurements is shown in Figure 3-30.

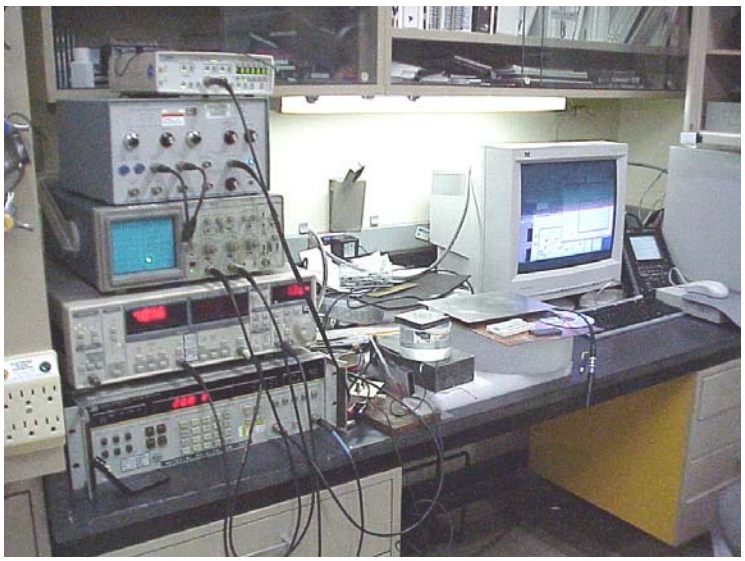

Figure 3-30. Laboratory components assembled for investigative EC/material response studies. This setup provides EC flaw detection capabilities similar to the commercial unit but allows greater latitude in signal analysis, data processing, probe design, and response modeling. Emphasis is on material properties evaluation as well as flaw detection.

Measurement of the frequency dependant complex impedance, both with the probe at free space and at the material surface, reveals that the influence of the sample is manifested in a convolution of shifts in the resonance frequency (f_o) and changes in the width of resonance (γ). This is consistent with our developed RL-C circuit model where an additional capacitor is introduced representing the stray capacitance due to the cables and instrumentation, which is usually neglected. Based on this, an increase in f_o represents a reduction in inductance and an increase in γ represents an increase in resistance in our model circuit. This response is schematically illustrated Figure 3-31 for the analogous cases of the probe over good and flawed surfaces. With the measured, frequency-dependent impedance response, a number of interesting material response properties can be described. The relation between variation of conductivity and the resultant variation between resonance frequency and width is already a well-known phenomenon in microwave resonance. In Figure 3-32 the resonance frequencies and the widths of the resonance at the full half-power level have been plotted for four samples of various conductivities (copper, aluminum, brass, and steel). The nature of the response is similar to that presented earlier obtained using the conventional (single frequency) inspection unit, however the orientation of the plot is altered. The sample variations

(slope of the response line) can be explained in the free electron theory by the equality of the surface resistance and surface reactance in the diffusion transport frequency range (Ref. 3). Also plotted are the variations in f_o and γ induced by changes in the spacing between the probe and sample (lift-off distance). Changes in sample conductivity result in a reduced range of resonance widths as the lift-off distance is increased. This pattern converges into the single point corresponding to the probe at free space (infinite separation distance). In contrast to this, in the conventional representation of eddy current data (z_r, z_i), all the points in Figure 3-14 would typically be mapped into points defining paths of various curvatures (some effects of this curvature are observable in the data presented earlier).

The plot in Figure 3-32 also shows experimental data for the effects that a "crack" feature has in the f_o vs γ plane. The change from the position of the "good" Cu point is a combination of conductivity effect and liftoff effect as mention before. Figure 3-33 shows the same data in a rescaled plot and details the "crack" response in copper (same specimen shown in Figure 3-4). The multiple data points represent repeated readings and the system "noise" associated with the measured impedance and resonant peak extraction. This noise (together with contributions from repeated probe placements) becomes one factor defining the measurement resolution or "detectibility limit" for a flaw feature. As the flaw signal comes closer to the unflawed material signal, a limit to flaw detectability will be reached. The previous plot has already shown how the effect of probe liftoff, or TPS thickness, can also be predicted in this manner.

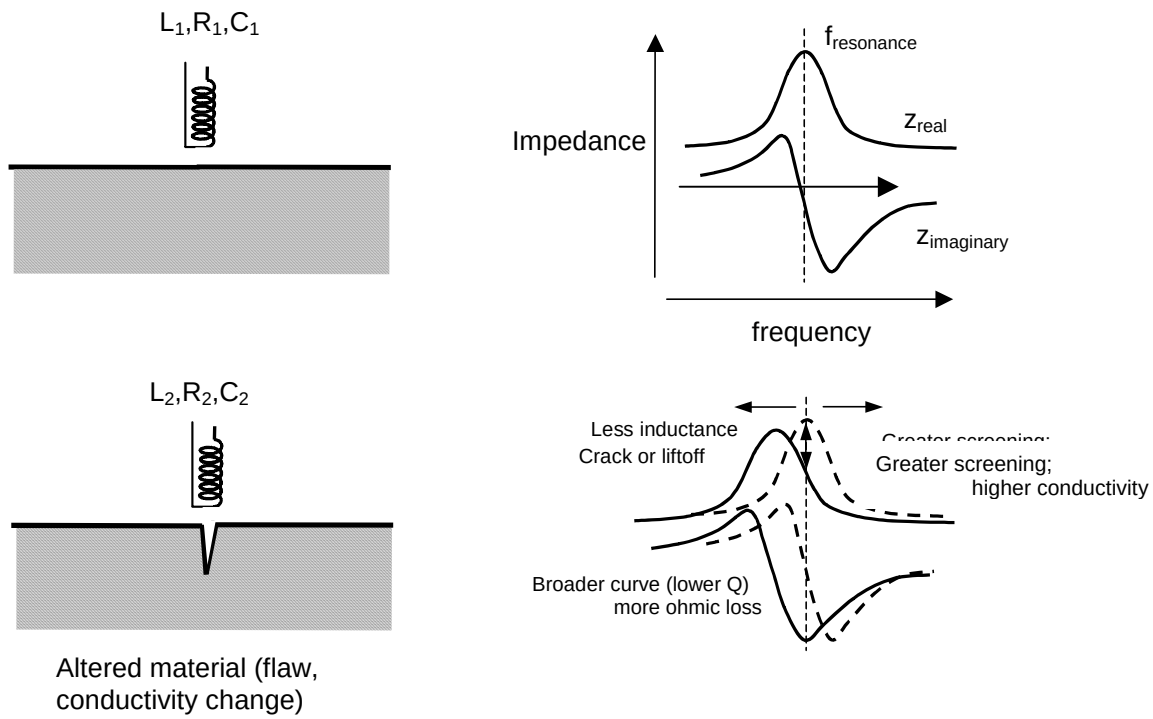

Figure 3-31. By measuring frequency-dependant complex impedance, the influence of the sample with and without a flaw is manifested in a shift in the resonance frequency and a change in the width of resonance.

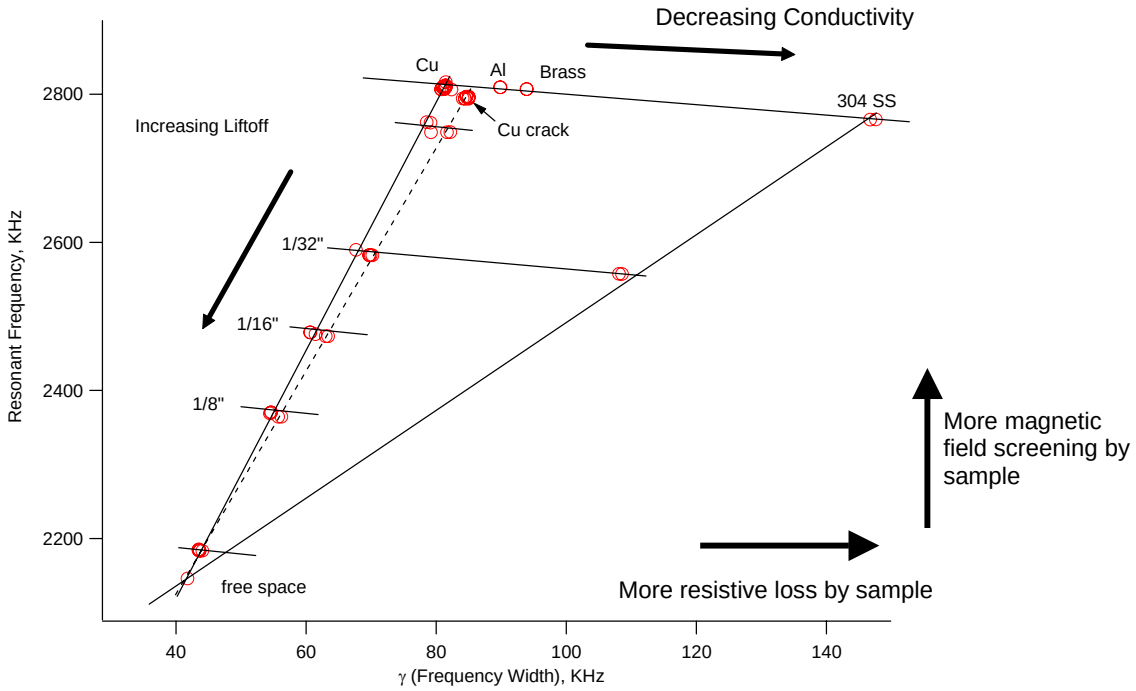

Figure 3-32. Presentation of eddy current signal response plotted as resonant frequency and frequency width, derived from swept-frequency impedance measurements. Systematic effects of conductivity variations and probe lift-off distance are clearly evident and can be extrapolated.

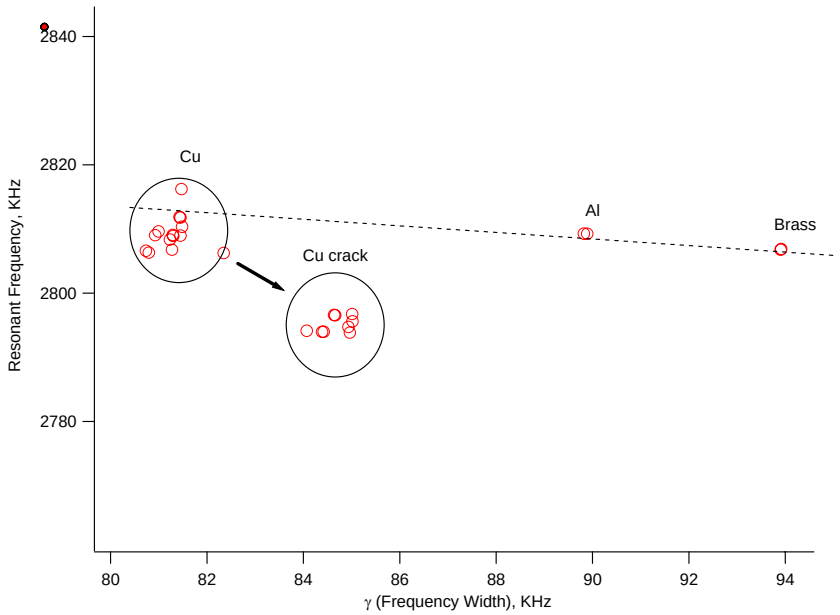

Figure 3-33. Enlargement of plot shown in prior figure. Scatter in measurement data will be important in defining the limit in liftoff or TPS thickness that can be sustained and still resolve the signal produced by the flaw.

It should be pointed out that these methods were performed on the fabricated crack of the re-joined split copper plate described earlier. The direction and slope of the impedance change in Figure 3-33 bears the same relationship to the "conductivity line" as the wide cracks in 6061-T6 Al obtained with the conventional testing unit. The "noise disk" is arbitrarily represented for the limited number of readings obtained in this example. This copper data, however, again show how rapidly resolution of the "crack" falls with probe lift-off. With the limited sampling of measurements shown in Figure 3-32, the "crack" impedance change begins to merge with the "good" surface at a lift-off distance near 1/8 inch. This is similar to the 0.12-in limit determined with the conventional testing unit.

The measurements obtained using this alternative technique have also employed eddy current probes that have been constructed in our laboratory. While many specialty probes can be designed for the unique demands of a particular inspection configuration, most probes selected for flat surface inspections are based on coil winding designs (frequently around a ferrite core) similar to the one shown in left of Figure 3-34. As well as being very selective in inspection area (high spatial resolution), this style of probe induces circular eddy currents that are equally sensitive (but not optimized) to all orientations of surface cracks (desirable for tight fillet welds, gear roots, etc). Another point is that much of the electromagnetic field is distributed above the specimen plane. One way to optimize the effect of the induced field (probe becomes more efficient, and a better detector) is to utilize a double-pole, or horseshoe-type ferrite core. This effectively directs the entirety of the field into the specimen half-plane. The resulting eddy currents are now highly unidirectional, concentrated within the poles of the core (as shown in the right of Figure 3-34). The advantage is that flaws oriented in one direction (or broken fibers in a conductive composite), will be selectively detected over other directions. Multiple scans in various directions can allow for the discrimination of flaw orientation in the inspected material. A photo of some of the laboratory-constructed probes is shown in Figure 3-35.

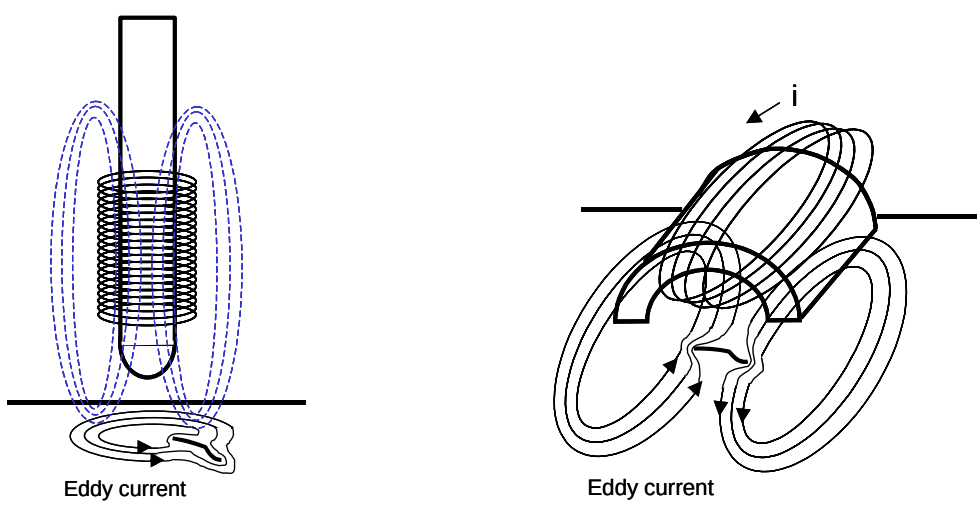

Figure 3-34. Contrast of coil design used in typical pencil probes (left) and horseshoe core that induces directional eddy currents that can be used to discriminate the orientation of specific flaws.

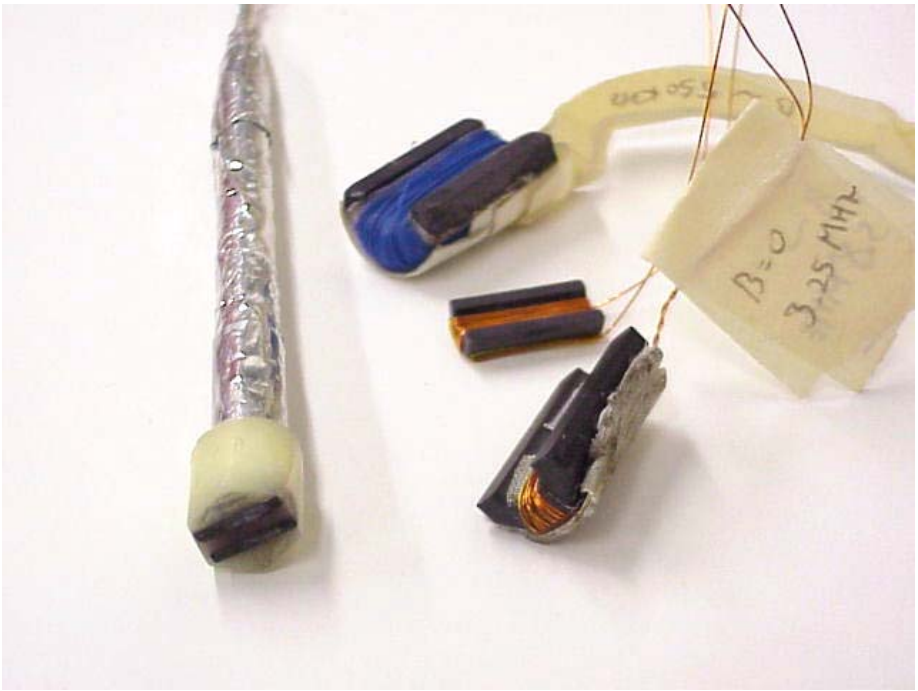

Figure 3-35. Laboratory constructed horseshoe probes used in the development of alternate eddy current approaches.

In addition to the clarity provided by these alternate approaches to conventional eddy current testing, this method of assessing the inductance change may facilitate many advanced eddy current NDE capabilities; for example:

- From measured lift-off data, the unwanted effect due to the variation of probe-to-sample distance can be filtered out in order to isolate conditions due to the sample alone.
- The nature of a defect can be determined by analyzing the signal in terms of the physical parameters (surface impedance or electrical conductivity).
- Two different sets of eddy current NDE data taken on the same sample can be compared by the translation of data into fundamental parameter space of surface resistance and surface reactance.
- Complex structural and material variations can be resolved by the comparison of data from many measurements with different settings of coil, spacers, or frequencies.

4. Summary of Results

An evaluation of eddy current inspection resolution for TPS covered substrates of 6061-T6 aluminum alloy and graphite epoxy composite materials was successfully performed through a series of practical measurements. For a matrix of flaws (surface cracks in the alloy and graduated impact damage in the composite), the sensitivity of the flaw detection signal to probe lift-off distance was used to establish the limit of TPS thickness beyond which flaw detection will be difficult to resolve. In this study, both EDM manufactured notches of finite length and novel split-plate coupons with variable width cracks of infinite length were used to characterize the impedance response change for one alloy/probe configuration. A sequence of increasing impact damage was produced in the composite material order to provide a range of flaw structures for eddy current detection. The resulting measurements showed that over the range of crack sizes investigated in the alloy, the limit in eddy current detection generally occurs when the lift-off, or TPS thickness, exceeds approximately 0.12 inches in height above the flaw. Although discrimination in crack shape was discerned by the specific impedance change measured at the alloy surface, the magnitude of the impedance signal can vary directly with the width and depth of the surface flaw. Results have been presented that show how signal strength attenuates with TPS thickness compared with the response at the bare surface for the various crack shapes investigated. In the case of the composite relatively light damage that cannot be detected by visual examination, was detected at the surface by eddy current inspection (effect of ply delamination). However, such subtle damage is difficult to detect at lift-off distances greater than 0.04 inches. For more severe damage that is quite evident by visual inspection (delamination with surface cracks and broken fiber damage), detection by eddy current is viable for a TPS thickness in the range of 0.12 inches. Lift-off distance provided a good corollary to TPS thickness if the TPS material is relatively hard and smooth. It was found that very soft materials, like non-coated cork, can be easily depressed with light pressure causing probe lift-off to contribute to the flaw signal. Despite the clear distinction between flaw and lift-off signatures, direct handheld inspection over the soft surface was abandoned in favor of a probe fixture.

5. Conclusions and Recommendations

An experimental investigation of the effect of TPS thickness on flaw detection capability was conducted using a limit number of flaw specimens and conventional eddy current methods. The results have provided an indication of the sensitivity of the inspection method for future RLVs structures that have a concern for assessing the health of structural components that remains covered by a thermal protection system. The results do not represent a rigorous evaluation of the detection limits of a specific NDE method (as in a probability-of-detection evaluation) for which a program of much wider scope and funding should be conducted. This study was intended to show how practical measurements could be undertaken that provide a background to the capabilities and limitation concerning the use of eddy current inspection on TPS-covered structures.

It is recommend that this study be used as a basis for future experimentation that can revisit some of the concerns raised in the course of this work. These concerns include the fidelity of the flaw specimen used in testing to model actual flaws that may be encountered in flight hardware. Limited resources of this study precluded the generation of specimen with actual fatigue-type flaws. Both the nature and quantity of test specimens should be enhanced in future efforts.

Finally, as an introductory study highlighting the concerns and limitations of NDE inspection processes for TPS-covered structures, a continuing effort should be directed toward similar overview-type, limited investigations, of alternate inspection methods.

.

6. Abbreviations and Symbols

AST	Office of Commercial Space Transportation
COTR	Contracting Officer's Technical Representative
deg	degree
EC	eddy current
EDM	electronic discharge machining
emf	electromagnetic field
eV	electron volt
f_o	resonant frequency
FAA	Federal Aviation Administration
ft	foot
fps	frames per second
g	width
γ	gamma
GHz	gigahertz
in	inch
kHz	kilohertz
lb	pound
MHz	megahertz
mm	millimeter
NDE	nondestructive evaluation
RF	radio frequency
RLV	reusable launch vehicle
S	standard penetration depth (eddy current)
s	second
TPS	thermal protection system
z_r, z_i	complex impedance

7. References

1. Esquivel, O., and Seibold, R. W., "Capabilities and Limitations of Nondestructive Evaluation Methods for Inspecting Components Beneath Thermal Protection Systems, Final Report, U. S. Department of Transportation Contract DTRS57-99-D-00062, Task 5.0, Aerospace Corporation Report. No. ATR-2004(5081)-1, July 30 2004.

2. Hull, B., and John, V., *Non-Destructive Testing*, Springer-Verlag New York, Inc. (1988).

3. Reitz, J. R., and Milford, F. J., *Foundations of Electromagnetic Theory*, Addison-Wesley Publishing Company, Reading, Massachusetts (1967).